

NACA RM A53D14



# RESEARCH MEMORANDUM

THE LOW-SPEED LIFT AND DRAG CHARACTERISTICS OF A  
SERIES OF AIRPLANE MODELS HAVING TRIANGULAR  
OR MODIFIED TRIANGULAR WINGS

By David Graham

Ames Aeronautical Laboratory  
Moffett Field, Calif.

~~CLASSIFICATION CHANGED~~

To Confidential

By authority of J. W. Crowley Date 12/1/53

CLASSIFIED DOCUMENT

This material contains information affecting the National Defense of the United States within the meaning of the espionage laws, Title 18, U.S.C., Secs. 793 and 794, the transmission or revelation of which in any manner to an unauthorized person is prohibited by law.

NATIONAL ADVISORY COMMITTEE  
FOR AERONAUTICS

WASHINGTON

June 15, 1953

~~CONFIDENTIAL~~  
~~RESTRICTED~~  
SECURITY INFORMATION

CLASSIFICATION CANCELLED

Authority NACA Res. 664 Date 4/6/56  
RN 99  
by MMH 4/27/56 See

[REDACTED]  
NATIONAL ADVISORY COMMITTEE FOR AERONAUTICSRESEARCH MEMORANDUMTHE LOW-SPEED LIFT AND DRAG CHARACTERISTICS OF A  
SERIES OF AIRPLANE MODELS HAVING TRIANGULAR  
OR MODIFIED TRIANGULAR WINGS

By David Graham

## SUMMARY

This report summarizes the lift and drag characteristics of a series of five low-aspect-ratio triangular-wing or modified triangular-wing airplane models. The series consists of three triangular wings of aspect ratios 2, 3, and 4, and two modified triangular wings of aspect ratio 2 having taper ratios of 0.20 and 0.33. Each of the wings was tested in combination with a high-fineness-ratio fuselage, a triangular vertical tail, and an unswept, all-movable horizontal tail. The Reynolds number of the tests varied from approximately 11 million for the aspect ratio 4 triangular wing to 15 million for the aspect ratio 2 triangular wing. The dynamic pressure of the tests was approximately 25 pounds per square foot and the Mach number was 0.13.

The experimental lift and drag characteristics of the five models are compared with existing theory. The relative merits of the models with respect to wing loading attainable for a given set of landing conditions are investigated.

The results of a comparison of the lift and drag characteristics of the five models indicate the following:

1. The effects of aspect ratio and taper ratio on the lift-curve slope at zero lift were as predicted by theory, and theory can be used to predict the lift-curve slope at zero lift for the subject wings and the increments of lift due to flap deflection at zero angle of attack for the aspect ratio 3 and 4 wings. For the aspect ratio 2 wings, the experimental increments of lift due to flap deflection were about 20 percent higher than the computed increments.

2. The experimental variation of drag due to lift for the wings with undeflected flaps and the variations given by inviscid potential-flow theory were in good agreement only up to lift coefficients of about 0.2. At the higher lift coefficients, experiment and separated-flow

[REDACTED]

[REDACTED]

theory are in closer agreement. Deflecting the flaps resulted in large decreases in drag at these higher lift coefficients which are of interest for low-speed flight.

A comparison of the five models on the basis of wing loadings indicates that the choice of a plan form that could carry the highest wing loading for any given landing speed would depend on the maximum permissible ground attitude. Another factor that influences this comparison is the fact that the ground effect for the triangular wings increases significantly with decreasing aspect ratio.

## INTRODUCTION

The low-speed aerodynamic characteristics at high Reynolds number of a systematic series of airplane models having wings of triangular and modified triangular plan forms have been reported in detail in references 1 to 6. Three triangular-wing models employing wings of aspect ratios 2, 3, and 4 were investigated to determine the effect of aspect ratio. The triangular wing of aspect ratio 2 together with two modified triangular wings having aspect ratios of 2 and taper ratios of 0.20 and 0.33 were used to determine the effect of taper ratio at a constant aspect ratio. Each of these wings was tested in combination with a high-fineness-ratio fuselage, a triangular vertical tail, and an unswept all-movable horizontal tail.

The results of tests of each of the five models were generally reported separately and without analysis of the results in order to expedite their publication. There is a need, therefore, for a summarization of the results, an evaluation of the relative merits of the models from the standpoint of their low-speed characteristics, and a determination of the applicability of theory for the prediction of the characteristics of similar models. It is the purpose of this report to accomplish the foregoing objective with respect to the lift and drag characteristics of the models. Some pitching-moment data are included herein, although it is not the purpose of this report to summarize and discuss the stability of the models.

## NOTATION

A	aspect ratio, $\frac{b^2}{S}$
b	wing span, ft
b <sub>t</sub>	horizontal-tail span, ft
c	wing chord, measured parallel to plane of symmetry, ft

$\bar{c}$	mean aerodynamic chord of wing, measured parallel to plane of symmetry, $\frac{\int_0^{b/2} c^2 dy}{\int_0^{b/2} c dy}$ , ft
$C_D$	drag coefficient, $\frac{D}{qS}$
$C_L$	lift coefficient, $\frac{L}{qS}$
$C_m$	pitching-moment coefficient, $\frac{M}{qS\bar{c}}$
$D$	total drag, lb
$h$	height of quarter-chord point of root chord of wing above the ground, ft
$i_t$	horizontal-tail incidence relative to the wing-chord plane, deg
$L$	total lift, lb
$L/D$	lift-drag ratio
$l_t$	distance from center-of-gravity location to pivot line of horizontal tail, ft
$M$	total pitching moment about the center of gravity, ft-lb
$q$	free-stream dynamic pressure, lb/sq ft
$S$	wing area, sq ft
$S_t$	horizontal-tail area, sq ft
$T$	thrust, lb
$V_h$	horizontal speed, mph
$V_v$	sinking speed, ft/sec
$W$	airplane weight, lb
$y$	lateral coordinate perpendicular to plane of symmetry, ft
$\alpha$	free-stream angle of attack with reference to the wing-chord plane, deg

$\alpha_g$	ground angle with reference to the wing-chord plane, deg
$\delta_f$	flap deflection, measured in a plane perpendicular to hinge line, deg
$\lambda$	taper ratio, $\frac{\text{tip chord}}{\text{root chord}}$

### MODELS

Drawings of the models are shown in figure 1, and figure 2 shows one of the models in the Ames 40- by 80-foot wind tunnel. The pertinent dimensional data are presented in table I and figure 1.

The wings having taper ratios of 0.20 and 0.33 were obtained by removing portions of the tips of the aspect ratio 3 and 4 triangular wings, respectively, such that the resulting aspect ratio of each was 2. The airfoil sections of all the wings, taken parallel to the model center line, were NACA 0005 sections modified by using a straight-line fairing from the 67-percent-chord station to the trailing edge. The ordinates of the airfoil section are given in table II. A further modification to the airfoil section was necessary for the aspect ratio 3 triangular wing and aspect ratio 2, taper ratio 0.20 wing. This additional modification, required because of the construction technique used, was located a considerable distance back of the leading edge and, hence, should have insignificant effect on the low-speed characteristics. The details of the modification can be found in references 5 and 6. The models were all equipped with single-slotted trailing-edge flaps. The flap plan forms are shown in figure 1. Further detailed descriptions and dimensions of the models are given in references 1 through 6.

### TEST CONDITIONS AND CORRECTIONS TO DATA

The Reynolds numbers of the tests, based on the mean aerodynamic chord, are listed in table III for the five models. The dynamic pressure of the tests was approximately 25 lb/sq ft and the Mach number was 0.13.

The data were corrected for wind-tunnel-wall effects and support-strut interference.

### RESULTS

The basic lift and drag characteristics of the five models, with and without the horizontal tails, are summarized herein. Although it is

beyond the scope of this report to analyze and discuss longitudinal stability, a limited amount of pitching-moment data for the five models is presented because of the influence of these data on trim lift and drag characteristics. The pitching-moment data for the models without the horizontal tails are referred to the quarter-chord point of the mean aerodynamic chord. In order to facilitate the discussion, the pitching-moment data for the complete models are referred to center-of-gravity locations for which a value of  $(dC_m/dC_L)_{C_L = 0}$  of -0.06 was obtained for each model when the trailing-edge flaps and the horizontal tail were undeflected. The center-of-gravity locations for the five complete models are listed in table IV.

Although all the models were tested with the horizontal tails located in various vertical positions, the data for the models with the horizontal tails included herein are limited to the case of the horizontal tail in the extended wing-chord plane. This position of the horizontal tail has been shown to give the best longitudinal stability at low speeds for all the models. For further information see references 1, 3, 5, and 6.

The basic lift, drag, and pitching-moment characteristics of the three triangular-wing models and three aspect ratio 2 wing models without the horizontal tails are presented in figures 3 and 4, respectively. The lift, drag, and pitching-moment characteristics of the complete triangular-wing models and the aspect ratio 2 wing models are presented in figures 5 and 6, respectively. These data are presented for the models with the horizontal tails set at  $0^\circ$  incidence.

## DISCUSSION

The discussion is divided into two main parts. The first part is concerned with an examination of the experimental data to show the effects of the various model configurations on important lift and drag parameters. In addition, comparisons of theoretical results with corresponding experimental results are made where possible. In the second part of the discussion, an evaluation is made of the relative merits of the various models with respect to wing loadings and thrust required to maintain a given landing speed and sinking speed.

### Examination of Experimental Results and Comparison With Theoretical Results

Lift due to angle of attack.— The effects of aspect ratio and taper ratio on the lift-curve slope at zero angle of attack of the triangular and aspect ratio 2 wing models are shown in figure 7. In addition to the

experimental variations shown for the wing-fuselage models, the theoretical values of lift-curve slope for the wings alone as given by the theory of reference 7 are included. The theoretical wing-alone values were used for the comparison since, as shown by the experimental results of references 8 and 3, the effect on the lift-curve slope of the addition of a fuselage to aspect ratio 2 and 4 triangular wings, respectively, was small. It therefore seems reasonable to assume that the effect of the addition of the fuselage to the other three wings is also small.

The correlation of the theoretical values of  $C_{L\alpha}$  with the experimental values indicates that the wing-alone theory of reference 7 can be used to predict the effects of aspect ratio and taper ratio on the lift-curve slopes of low-aspect ratio wing-fuselage configurations at low angles of attack.

As will be noted from the basic lift curves (figs. 3 and 4) for the various models, the values of lift-curve slope at zero lift coefficient are not generally applicable in estimating the lift at angles of attack required for landing. A measure of the departure of the lift-curve slope from linearity is shown by figure 8, wherein the ratio of  $C_L / [(C_{L\alpha})_{C_L = 0} \times \alpha]$  is plotted as a function of angle of attack.

$C_{L_{max}}$  and  $\alpha$  for  $C_{L_{max}}$ .- Maximum lift coefficient is only of minor interest for most of the wings because of the large angles of attack involved. Hence, no special effort was made to determine the values of  $C_{L_{max}}$  for all models, the only values determined being those for the aspect ratio 3 and 4 triangular wings. The values of  $C_{L_{max}}$  and  $\alpha$  for  $C_{L_{max}}$  which were determined are shown in figure 9 along with values for an aspect ratio 2 wing alone obtained from reference 9.

The value of  $C_{L_{max}}$  for the aspect ratio 2 wing alone is believed to be indicative of  $C_{L_{max}}$  for the wing-fuselage model; this belief is based on the data of fuselage effects which are given in reference 8. Small-scale tests on wing-alone models (refs. 10 and 11) indicate that the  $C_{L_{max}}$  for triangular wings would be a maximum for the aspect ratio 2 wings. For an aspect-ratio range above 4, the rate of change of  $C_{L_{max}}$  with aspect ratio would be reduced.

The effect of taper ratio on the  $C_{L_{max}}$  of aspect ratio 2 wings is indicated by the shape of the lift curves at the highest  $\alpha$ 's reached (see fig. 4(a)). For these wings,  $C_{L_{max}}$  would decrease with increasing values of taper ratio.

Lift due to flap deflection.- The variation of flap effectiveness with aspect ratio of the triangular-wing models, and with taper ratio of the aspect ratio 2 models cannot be determined from the experimental data, since the flap plan form and ratio of flap area to wing area was not the same for all models. It is possible, however, to compare the experimental and theoretical increments of lift due to flap deflection of each model to determine the applicability of theory. This comparison is provided in figure 10 where the increments of lift obtained at  $0^\circ$  angle of attack for flap deflections of  $40^\circ$  are compared with those computed by the theory of reference 12.<sup>1</sup> Also included in figure 10 are the experimental and computed increments of lift due to flaps obtained for two wing-alone, aspect ratio 2 wings. One of these wings had the slotted, constant-percent-chord flap used on the wing-fuselage model and extended to the wing center line. The second wing had a constant-chord, sealed, 20-percent-wing area, plain flap with the flap deflected only  $10^\circ$  (data from ref. 9).

The theoretical values were determined by the following method: Although the simplified lifting-surface theory of reference 12 is for wings alone, it was applied to the wing-fuselage combination, in which case the assumption was made that only the actual flap area was effective (i.e., the flap was not assumed to extend across the fuselage). The two-dimensional values of the parameter  $d\alpha/d\delta$  shown in figure 11 were used for the calculation.

The comparisons of the theoretical flap lift increments with the measured values show the following results: There is good agreement between the theoretical and experimental values for the triangular wings of aspect ratios 3 and 4; whereas, for all the wings of aspect ratio 2, the experimental values were about 20 percent higher than the theoretical values. As noted in reference 12, this discrepancy is probably due to the use of values of  $d\alpha/d\delta$  which were obtained in two-dimensional tests and applied to low-aspect-ratio wings which approach the lower limit of aspect ratios for which the  $d\alpha/d\delta$  concept has been judged acceptable. The assumption that the flaps did not extend across the fuselage made in the calculation of the increments of lift due to flap deflection is shown to be a good one by the results shown in figure 10, where the deviation of the increment of  $C_L$  computed for the wing-alone and the wing-fuselage model having the constant-percent-chord flap are approximately the same.

Increments of lift at an angle of attack of  $0^\circ$  do not always give a reliable indication of the flap effectiveness at the higher angles of attack. This is shown in figure 12 wherein the ratio of the increment of lift at each angle of attack to the increment of lift at  $0^\circ$  angle of attack is plotted as a function of angle of attack. Up to an angle of attack of  $16^\circ$ , the ratios for the aspect ratio 2 wings were equal to or

---

<sup>1</sup>The assumption was made in the calculation that the increment of lift due to flap deflection was linear up to a flap deflection of  $40^\circ$ . The results of reference 1 show this to be the case for the aspect ratio 2 triangular wing.

greater than 1, while the ratio for the aspect ratio 3 and 4 wings decreased, so that at  $16^\circ$  angle of attack there were losses from the value of  $\Delta C_L$  at  $\alpha = 0^\circ$  of approximately 20 percent and 40 percent, respectively.

Drag due to lift.- The span efficiency factor  $e$  is commonly used to compare the experimental and theoretical drag due to lift. This parameter is of little value for the present wings because the variation of  $C_D$  with  $C_L^2$  for each of the wings was not linear, as has been the case for wings of conventional plan form. It appears that the best method of comparison for the present wings is on the basis of the degree of agreement between experimental and theoretical variations of  $C_D$  with  $C_L^2$ .

In order to indicate the degree of agreement, experimental and theoretical variations for the various models are given in figure 13. Two types of theoretical variations are shown. One variation,  $C_{D_i}$  with  $C_L^2$  given by the theory of reference 7, is for the condition of unseparated or inviscid potential flow. The other variation,  $C_L \tan \alpha$  with  $C_L^2$ , is for a condition of completely separated flow on the wing such that the resultant force is normal to the chord plane. Both theoretical variations are for the wing alone with undeflected flaps, and the experimental variations shown are for the wing-fuselage model with flaps undeflected and deflected  $40^\circ$ . The experimental value of the drag coefficient at  $C_L = 0$ ,  $C_{D_0}$ , for the models with undeflected flaps was assumed to be the profile drag through the lift range.

The degree of agreement between the experimental variation for each wing with undeflected flaps and the corresponding two theoretical variations is dependent upon the lift coefficient. Only at low lift coefficients (less than 0.2) was there good agreement between experiment and the inviscid potential theory. At the higher lift coefficients, which are of interest for low-speed flight, experiment and the completely separated-flow theory are in closer agreement. This is indicated, for example, in the following table which gives ratios of experimental  $C_D$  to the  $C_D$  given by the separated-flow theory, for a lift coefficient of 0.9:

Wing model	$C_{D_{exp}} / (C_{D_0} + C_L \tan \alpha)$
A, 4; $\lambda$ , 0	0.91
A, 3; $\lambda$ , 0	.82
A, 2; $\lambda$ , 0	.85
A, 2; $\lambda$ , 0.20	.82
A, 2; $\lambda$ , 0.33	.90

Also of importance to note from the variations of  $C_D$  with the square of  $C_L$  is the large effect of the flaps. At values of  $C_L$  of interest for low-speed flight, large reductions in  $C_D$  resulted from deflecting the flaps. These reductions of drag with the flaps deflected resulted from a variation of  $C_D$  with the square of  $C_L$  that was close to that given by the inviscid potential theory over a wider  $C_L$  range than was the case for flaps undeflected.

Trim lift and drag characteristics.— The effects of aspect ratio of the triangular-wing models, and taper ratio of the aspect ratio 2 wing models on trim  $C_L$  with a 6-percent static margin are shown in figures 14 and 15, respectively; the aspect-ratio effects, and the taper-ratio effects on trim  $L/D$  are shown in figures 16 and 17, respectively. The effects shown are directly those of aspect ratio and taper ratio only for the flaps-undeflected case and for the given static margin. With the flaps deflected there were also effects of varying the flap plan form and varying the ratio-of-flap area to wing area.

The loss in  $\Delta C_L$  at  $\alpha = 0^\circ$  which results from trimming out the increments of  $C_m$  due to flap deflection is shown in figure 18. For a 6-percent static margin, the reduction in  $\Delta C_L$  at  $\alpha = 0^\circ$  varied from approximately 15 percent for the aspect ratio 4 triangular-wing model to 24 percent for the aspect ratio 2 triangular-wing model.

In order to eliminate the effects of differences in flaps, estimates have been made of the trim lift and drag characteristics of the models with flaps of the same plan form and same ratio-of-flap area to wing area. The assumed models had the ratios of dimensions of the components used for the triangular-wing models. Full-span, constant-chord, 20-percent-wing-area flaps were assumed. Increments of  $C_L$  due to  $40^\circ$  flap deflection were computed by the use of the theory of reference 12 and corrected by factors established from the experimental data (e.g., ratios indicated by figs. 10, 12, and 18).

The drag coefficients were computed in the following manner: The experimental increments of  $C_D$  and  $C_L^2$  obtained at a given angle of attack for a  $40^\circ$  deflection of the flaps of each model were used to compute the drag due to lift. The near linear curve of  $\Delta C_D$  versus  $\Delta(C_L^2)$  thus obtained was extrapolated to the higher  $C_L$ 's for the assumed flaps. An increment of drag coefficient due to landing gears was also included. For the type of gear considered this incremental drag coefficient varied from 0.026 at  $\alpha = 0^\circ$  to a value of zero at the maximum angle of attack and is based on unpublished data from the Ames 40- by 80-foot wind tunnel. The computed lift curves and lift-drag ratios are shown in figures 19 and 20, respectively.

The effects of aspect ratio and taper ratio indicated by the estimated characteristics are qualitatively the same as those indicated by

the experimental characteristics for the actual flaps used. Since, however, the areas of the assumed flaps were larger than the areas of the tested flaps, there are quantitative differences, as are indicated by the following table which shows values of trimmed  $C_L$  and  $L/D$  at an assumed landing angle of attack of  $16^\circ$ .

Model	Experimental for actual flaps		Estimated for assumed flaps	
	$C_L$	$L/D$	$C_L$	$L/D$
$A = 4, \lambda = 0$	1.20	3.1	1.37	2.7
$A = 3, \lambda = 0$	1.21	3.2	1.41	2.9
$A = 2, \lambda = 0$	1.04	2.9	1.27	2.4
$A = 2, \lambda = 0.20$	1.22	3.1	1.38	2.9
$A = 2, \lambda = 0.33$	1.29	3.1	1.45	2.7

It is interesting to note that the aspect ratio 2, taper ratio 0.33 wing had the highest value of  $C_{L_{trim}}$  at the assumed landing angle of attack.

The values of  $C_{L_{trim}}$  given for the same angle of attack are not necessarily indicative, however, of those for a given ground attitude because of ground effects and effects of finite values of sinking speed. Therefore, these effects will be considered in the following section of the report.

#### Evaluation of Landing Performance of the Various Models

This section of the report compares the landing performance of the various models in terms of attainable wing loading and the thrust required to maintain a given landing speed and sinking speed.

Relative merits of the models at a given landing speed and sinking speed.— A comparison of the models on a basis of attainable wing loadings at various ground angles is shown in figure 21. The wing loadings were computed assuming the following conditions:

1. Sinking speed  $V_V$  is zero, thus making the ground angle equal to the angle of attack.
2. Horizontal speed  $V_H$  is 120 mph.
3. Model is equipped with the assumed 20-percent-area flaps deflected  $40^\circ$ .

4. Sufficient thrust to maintain the specified speeds is provided along an axis formed by the intersection of the model plane of symmetry and the wing-chord plane. These thrusts are shown in figure 21 as required thrust per square foot of wing area versus wing loading.

5. Static margin at  $C_L = 0$  is 6 percent.

Included in figure 21 are the wing loading and thrust curves for a tailless, aspect ratio 2.31, triangular-wing model. The data for the tailless model were obtained from references 1 and 13.

Up to an angle of attack of  $12.5^\circ$ , the aspect ratio 4 triangular-wing model could carry the highest wing loading and would require the least amount of thrust for those wing loadings. In the range of angles of attack from  $12.5^\circ$  to  $18^\circ$ , the aspect ratio 2, taper ratio 0.33 model could carry the highest wing loadings, while it appears that at angles of attack higher than  $18^\circ$ , the aspect ratio 3 triangular-wing model would be able to carry the highest wing loadings.

Throughout the angle-of-attack range the aspect ratio 2 triangular-wing model with the horizontal tail was capable of carrying from 20 to 30 lb/sq ft more wing loading than the tailless model. In addition, for wing loadings above 30 lb/sq ft, the model with the horizontal tail required less thrust to maintain the specified flight conditions than did the tailless model.

The fact that these comparisons are only for one specified low-speed flight condition should be borne in mind. Any advantages of one configuration over another at this specified flight condition may be overshadowed by comparisons of the characteristics at high speed. Another point is that these comparisons were made for an arbitrarily chosen static margin of 6 percent for all models. Changes in static margin would alter the comparisons of the relative merits of the models.

Effect of sinking speed.- One condition, neglected in the foregoing calculated results, that could make significant changes in the attainable wing loadings is the effect of sinking speed. The major effects of increasing the sinking speed, while holding the horizontal speed constant, would be reductions in the values of  $\alpha_g$  and  $T/S$  which would be required for a given wing loading. For a given sinking speed, the changes in  $\alpha_g$  and  $T/S$  for all the models would be approximately the same. As an example of the changes in  $\alpha_g$  and  $T/S$  that would result from an increase in sinking speed, the variation of attainable wing loadings and required thrusts are shown in figure 22 for the aspect ratio 2 triangular-wing model for three assumed sinking speeds. It will be noted that for a given wing loading, a 10 ft/sec increase in sinking speed results in a reduction of  $\alpha_g$  of approximately  $3^\circ$  and reductions of  $T/S$  from 2 to 3 lb/sq ft. Since the maximum wing loading a model could carry, assuming no flare in the landing procedure, is limited by the maximum

lift coefficient of that model, there would be no change in maximum wing loading due to a change in sinking speed.

Effect of proximity to the ground.— Another condition that could make a significant change in the attainable wing loading is the effect of proximity of the model to the ground, or ground effect. The effect of proximity to the ground was considered for the three triangular-wing models. The theory of reference 14 was used for the calculation of ground effect. The theory was substantiated by a limited comparison of experimental (unpublished data) and calculated ground effects for low-aspect-ratio swept-wing airplane models. The following assumptions were made for the calculations:

1. Height of the quarter chord of the root chord above the ground is 7 feet.
2. The downwash at the horizontal tail is zero since the tail is in the proximity of the ground.
3. Flaps are deflected  $40^\circ$  and there is no change in flap effectiveness in the presence of the ground.
4. The sinking speed  $V_v$  is zero.
5. Horizontal speed  $V_h$  is 120 mph.
6. Sufficient thrust is provided to maintain conditions 4 and 5 above.

The results of these calculations for the triangular-wing models are given in figure 23 and show that the ground effect increases with decreasing aspect ratio. At  $16^\circ$  angle of attack the maximum wing loading of the aspect ratio 2 wing was increased from 52.5 to 58.8 lb/sq ft, a gain of 12 percent. At the same angle of attack, the wing loading of the aspect ratio 3 wing was increased from 57.3 to 59.7 lb/sq ft, a gain of 4 percent, while there was a slight loss for the aspect ratio 4 wing. As a result of the greater ground effect for the aspect ratio 2 wing than that for the aspect ratio 3 wing, the aspect ratio 2 triangular wing is capable of carrying wing loadings equal to those for the aspect ratio 3 wing at angles of attack above  $18^\circ$ . It is thus evident that, if a choice of an optimum configuration is to be made on the basis of the maximum possible wing loadings that could be carried at landing, the effect of the proximity of the ground should be determined for the configurations to be compared.

## CONCLUDING REMARKS

The results of a comparison of the lift and drag characteristics of five airplane models having triangular or modified triangular wings indicate the following:

1. The effects of aspect ratio and taper ratio on the lift-curve slope at zero lift are as predicted by theory, that is, increasing lift-curve slope with increasing aspect ratio for the triangular wings and increasing lift-curve slope with increasing taper ratio for the aspect ratio 2 wings.
2. Available theory can be used to predict the increments of lift due to flap deflection at zero angles of attack for the aspect ratio 3 and 4 wings. For the aspect ratio 2 wings, the experimental increments of lift due to flap deflection were about 20 percent higher than the computed increments.
3. For the three triangular wings tested, the maximum lift coefficient decreased with increasing aspect ratio. For the three aspect ratio 2 wings, a decrease in maximum lift coefficient with increasing taper ratio is indicated.
4. The experimental variation of drag due to lift for the wings with undeflected flaps and the variations given by inviscid potential-flow theory were in good agreement only up to a lift coefficient of about 0.2. At higher lift coefficients, experiment and theory for completely separated flow are in closer agreement. For the subject wings at a lift coefficient of 0.9, the experimental drag coefficient varied from 82 to 91 percent of the drag coefficient given by separated-flow theory. Deflecting the flaps resulted in large reductions in drag through the lift-coefficient range of interest for low-speed flight. For this condition the experimental variation of drag with lift appears to be in much better agreement with the inviscid potential-flow theory than does the variation for the wing with flaps undeflected.

The results of comparing the five complete airplane models on the basis of attainable wing loadings at various angles of attack show the following:

1. The choice of a plan form that could carry the highest wing loading for any given landing speed would depend on the maximum permissible ground attitude. Calculation of the wing loadings for a fixed horizontal speed of 120 mph and assuming no ground effect show that at the lowest angles of attack, the aspect ratio 4 triangular wing could carry the highest wing loadings. Through the middle and high range of angles of attack, the aspect ratio 2, taper ratio 0.33 and aspect ratio 3 triangular wings, respectively, could carry the highest wing loadings.

2. The ground effect for the triangular wings increases with decreasing aspect ratio, enabling the aspect ratio 2 triangular wing to equal the maximum wing-loading capability of the aspect ratio 3 triangular wing at the higher angles of attack.

Ames Aeronautical Laboratory  
National Advisory Committee for Aeronautics  
Moffett Field, Calif.

#### REFERENCES

1. Graham, David, and Koenig, David G.: Tests in the Ames 40- by 80-foot Wind Tunnel of an Airplane Configuration With an Aspect Ratio 2 Triangular Wing and an All-Movable Horizontal Tail - Longitudinal Characteristics. NACA RM A51B21, 1951.
2. Graham, David, and Koenig, David G.: Tests in the Ames 40- by 80-foot Wind Tunnel of an Airplane Configuration With an Aspect Ratio 2 Triangular Wing and an All-Movable Horizontal Tail - Lateral Characteristics. NACA RM A51L03, 1952.
3. Graham, David, and Koenig, David G.: Tests in the Ames 40- by 80-foot Wind Tunnel of an Airplane Configuration With an Aspect Ratio 4 Triangular Wing and an All-Movable Horizontal Tail - Longitudinal Characteristics. NACA RM A51H10a, 1951.
4. Franks, Ralph W.: Tests in the Ames 40- by 80-foot Wind Tunnel of an Airplane Model With an Aspect Ratio 4 Triangular Wing and an All-Movable Horizontal Tail - High-Lift Devices and Lateral Controls. NACA RM A52K13, 1953.
5. Koenig, David G.: Tests in the Ames 40- by 80-foot Wind Tunnel of an Airplane Configuration With an Aspect Ratio 3 Triangular Wing and an All-Movable Horizontal Tail - Longitudinal and Lateral characteristics. NACA RM A52L15, 1953.
6. Franks, Ralph W.: Tests in the Ames 40- by 80-foot Wind Tunnel of Two Airplane Models Having Aspect Ratio 2 Trapezoidal Wings of Taper Ratios 0.33 and 0.20. NACA RM A52L16, 1953.
7. DeYoung, John, and Harper, Charles W.: Theoretical Symmetric Span Loading at Subsonic Speeds for Wings Having Arbitrary Plan Form. NACA Rep. 921, 1948.
8. Anderson, Adrien E.: An Investigation at Low Speed of a Large-Scale Triangular Wing of Aspect Ratio 2.- III. Characteristics of Wing with Body and Vertical Tail. NACA RM A9H04, 1949.

9. Graham, David: Chordwise and Spanwise Loadings Measured at Low Speeds on a Large Triangular Wing Having an Aspect Ratio of 2 and a Thin Subsonic-Type Airfoil Section. NACA RM A50A04a, 1950.
10. Lange and Wacke: Test Report on Three- and Six-Component Measurements on a Series of Tapered Wings of Small Aspect Ratio (Partial Report: Triangular Wing). NACA TM 1176, 1948.
11. Tosti, Louis P.: Low-Speed Static Stability and Damping-in-Roll Characteristics of Some Swept and Unswept Low-Aspect-Ratio Wings. NACA TN 1468, 1947.
12. DeYoung, John: Theoretical Symmetric Span Loading Due to Flap Deflection for Wings of Arbitrary Plan Form at Subsonic Speeds. NACA Rep. 1071, 1952 (Supersedes NACA TN 2278).
13. Anderson, Adrien E.: Chordwise and Spanwise Loadings Measured at Low Speed on Large Triangular Wings. NACA RM A9B17, 1949.
14. Tani, Itiro, Taima, Masuo, and Simidu, Sodi: The Effect of Ground on the Aerodynamic Characteristics of a Monoplane Wing. Aeronautical Research Institute, Tokyo Imperial University, Rep no. 156, 1937.

TABLE I.- GEOMETRIC DATA OF MODELS

Wings					
Aspect ratio	4	3	2	2	2
Taper ratio	0	0	0	.20	.33
Area, sq ft	312.50	313.76	312.50	301.20	277.77
Span, ft	35.36	30.65	25.00	24.52	23.57
$\bar{c}$ , ft	11.78	13.65	16.67	14.11	12.77
Flap area (total movable), sq ft	37.43	37.43	37.44	37.43	37.43
Flap chord, ft or fraction c	1.96	1.96	0.2084c	1.96	1.96
Horizontal tails					
$S_t/S$	0.246	0.245	0.246	0.255	0.277
$b_t/b$	.521	.602	.738	.752	.782
$l_t/\bar{c}$ (moment center given in table IV)	1.735	1.550	1.161	1.584	1.716
Aspect ratio	4.4	4.4	4.4	4.4	4.4
Taper ratio	.46	.46	.46	.46	.46
Fuselage					
Length, ft	56.16	56.16	56.16	56.16	56.16
Maximum diameter, ft	4.49	4.49	4.49	4.49	4.49
Fineness ratio	12.5	12.5	12.5	12.5	12.5
Vertical tail					
Exposed area, sq ft	52.57	52.57	52.57	52.57	52.57
Aspect ratio	1	1	1	1	1
Taper ratio	0	0	0	0	0

NACA

TABLE II.- COORDINATES OF THE MODIFIED NACA 0005 SECTION

Station, % c	Ordinate, % c
0	0
1.25	.789
2.50	1.089
5.00	1.481
7.50	1.750
10.00	1.951
15.00	2.228
20.00	2.391
25.00	2.476
30.00	2.501
40.00	2.419
50.00	2.206
60.00	1.902
67.00	1.650
70.00	1.500
80.00	1.000
90.00	.500
100.00	0

L.E. radius: 0.275 % c



TABLE III.- REYNOLDS NUMBERS FOR THE VARIOUS MODELS

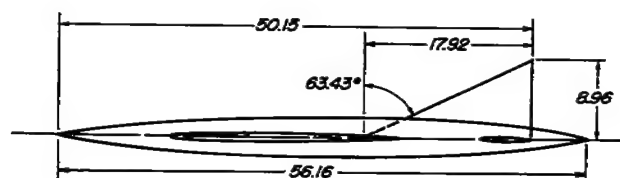
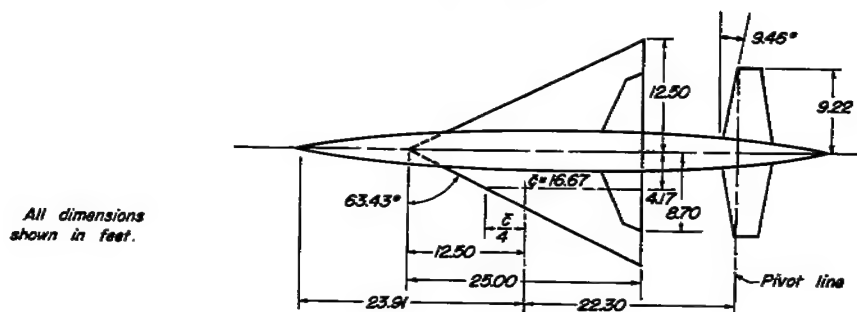
Aspect ratio	Taper ratio	Reynolds number
4	0	$10.9 \times 10^6$
3	0	$12.8 \times 10^6$
2	0	$14.6 \times 10^6$
2	0.20	$13.0 \times 10^6$
2	0.33	$11.4 \times 10^6$



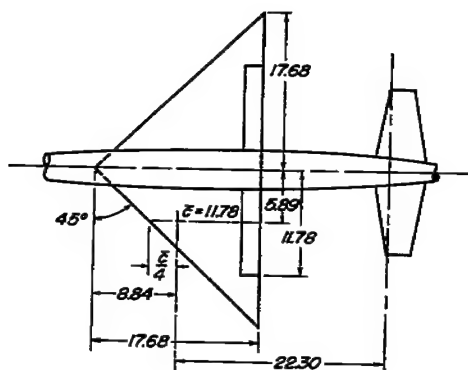
TABLE IV.- CENTER-OF-GRAVITY LOCATIONS FOR THE VARIOUS MODELS WITH THE HORIZONTAL TAILS

Aspect ratio	Taper ratio	Center-of-gravity location, % $\bar{c}$
4	0	40.8
3	0	43.6
2	0	42.6
2	0.20	36.9
2	0.33	33.8

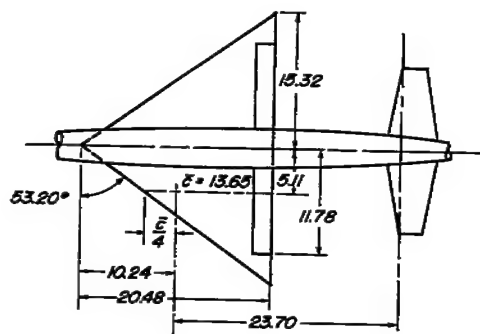




(a) A, 2



(b) A, 4



(c) A, 3

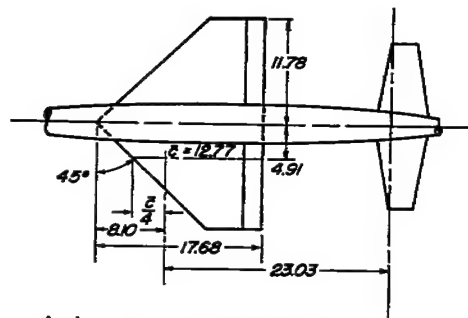
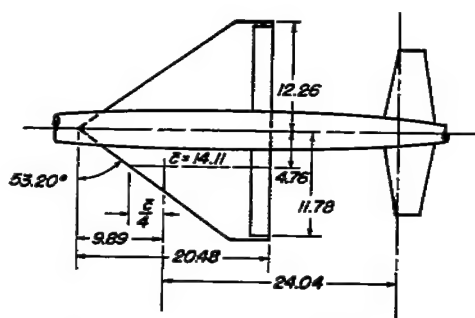
(d) A, 2;  $\lambda$ , 0.33(e) A, 2;  $\lambda$ , 0.20

Figure 1.- Geometric details of the models.



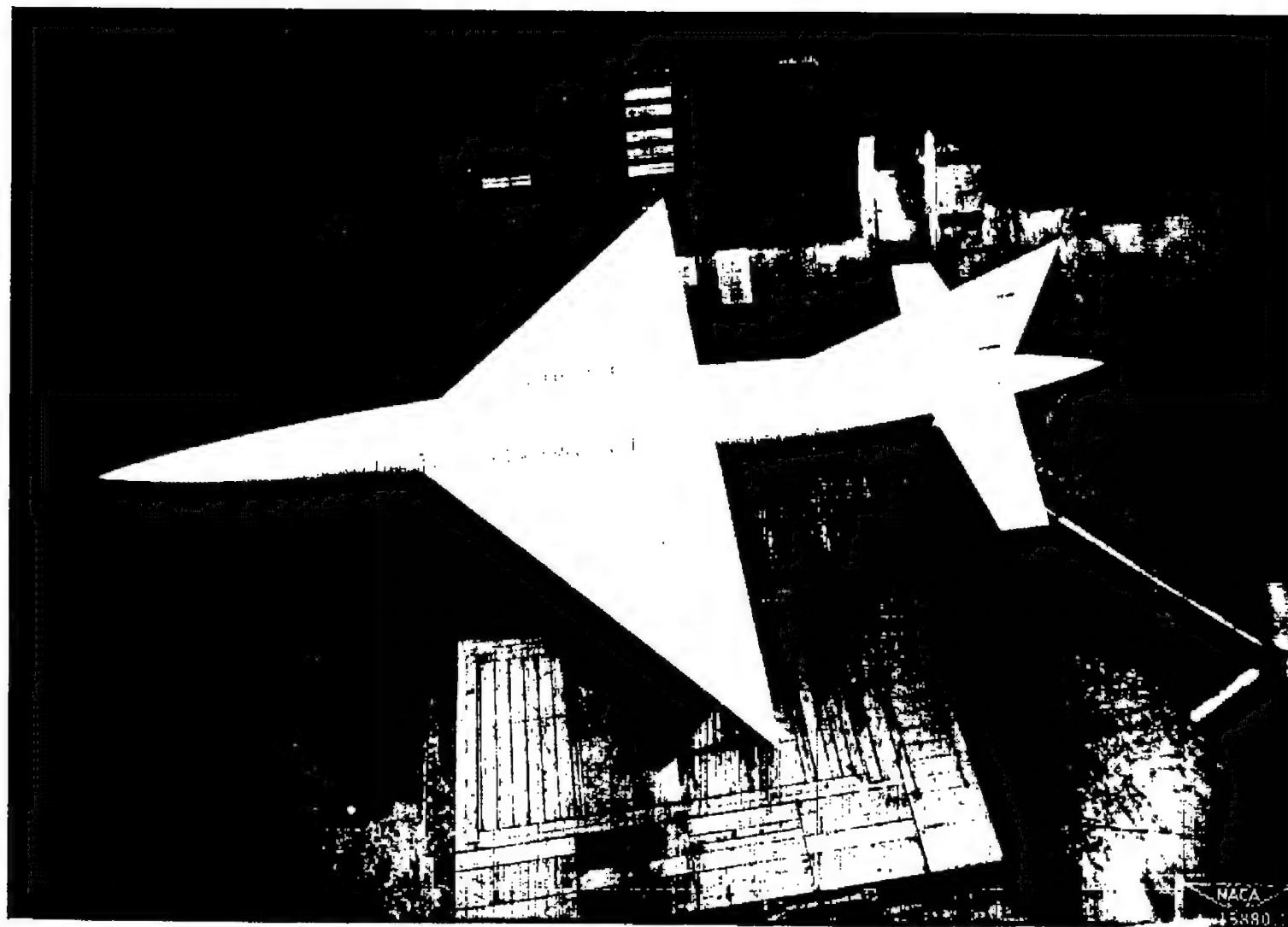


Figure 2.- The aspect ratio 4, triangular-wing model as mounted in the Ames 40- by 80-foot wind tunnel.

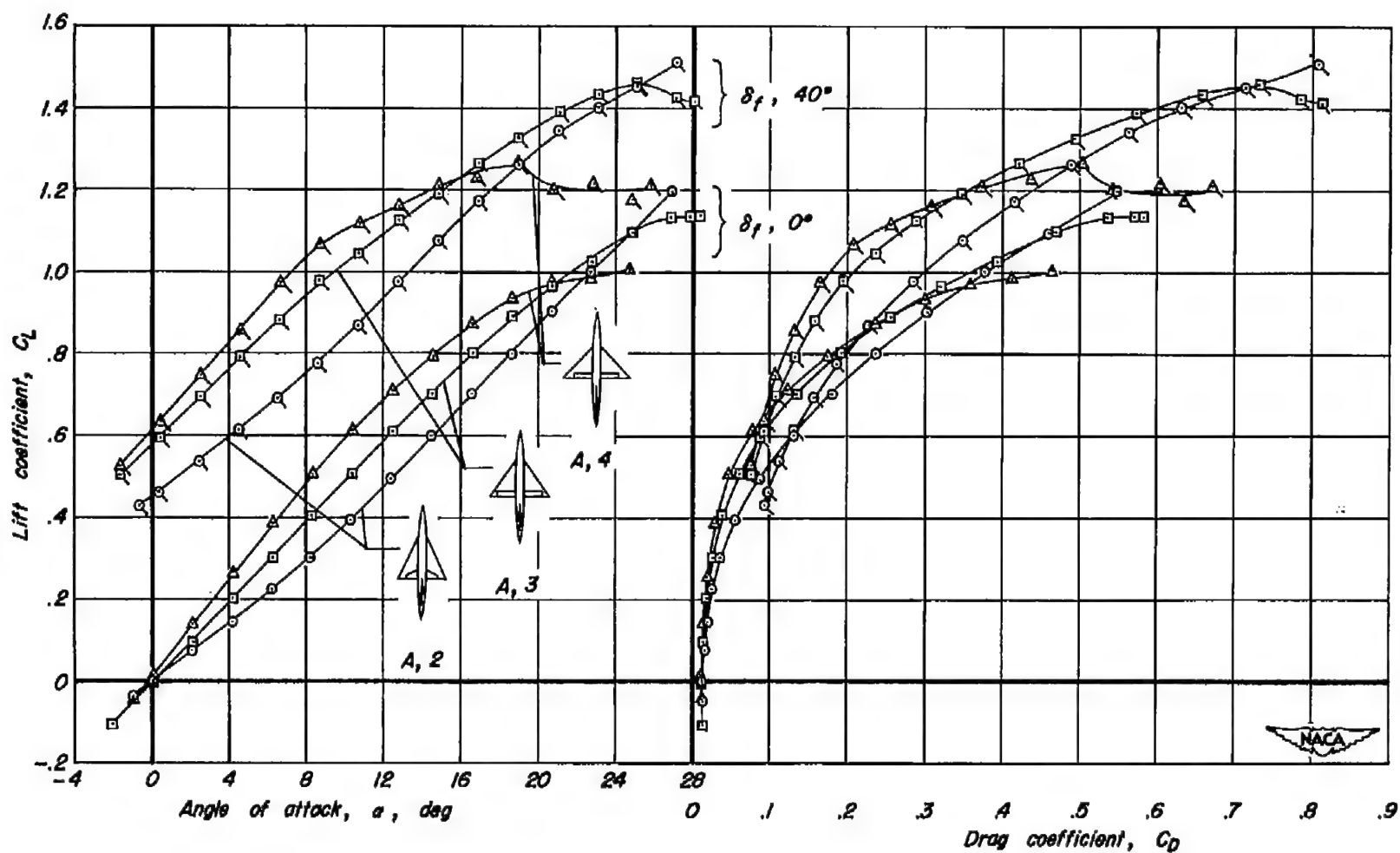
(a)  $C_L$  vs  $\alpha$ ,  $C_D$ 

Figure 3.- Longitudinal characteristics of the three triangular-wing models. Horizontal tail off; c.g.,  $0.25\bar{c}$ .

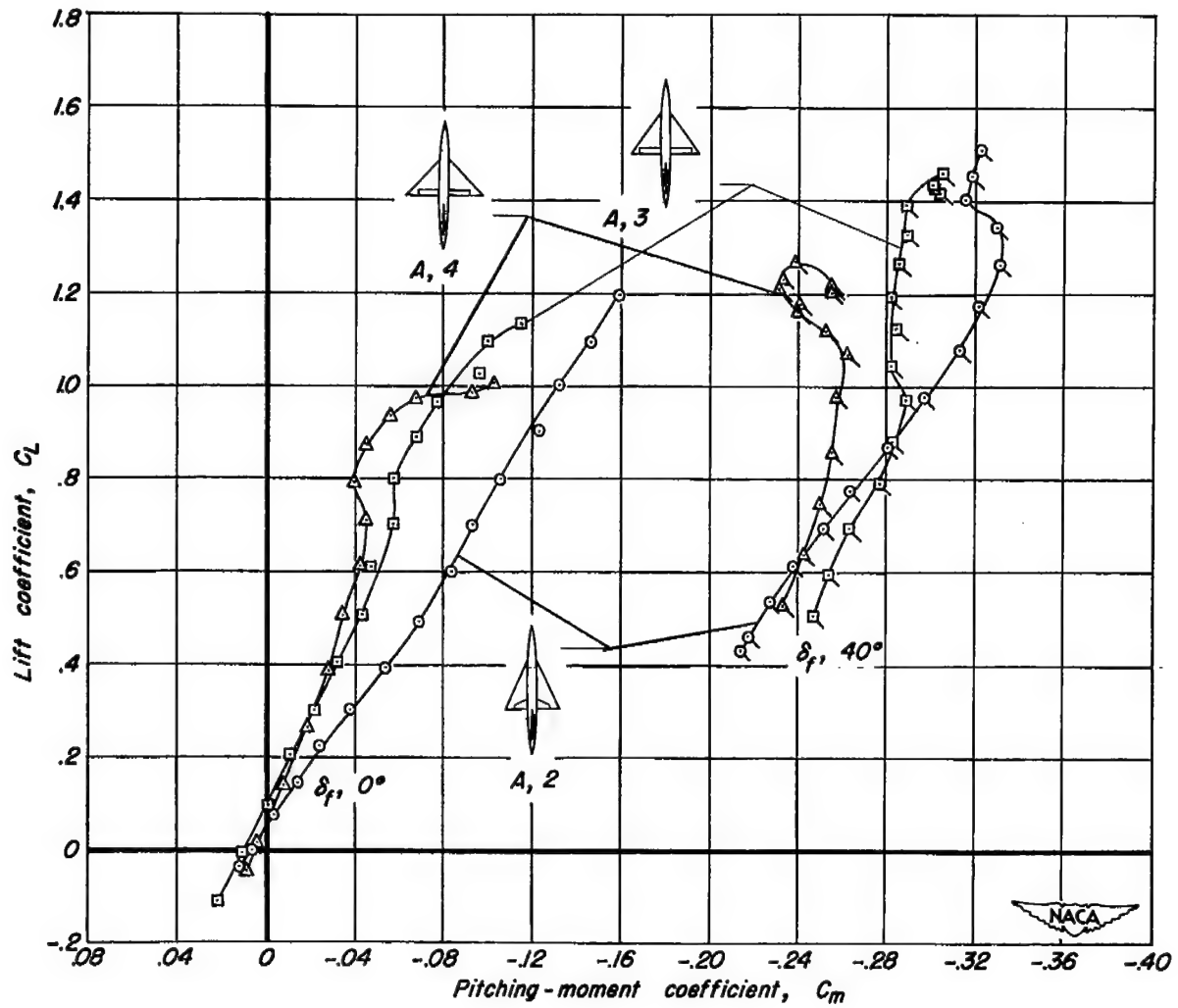
(b)  $C_L$  vs  $C_m$ 

Figure 3.- Concluded.

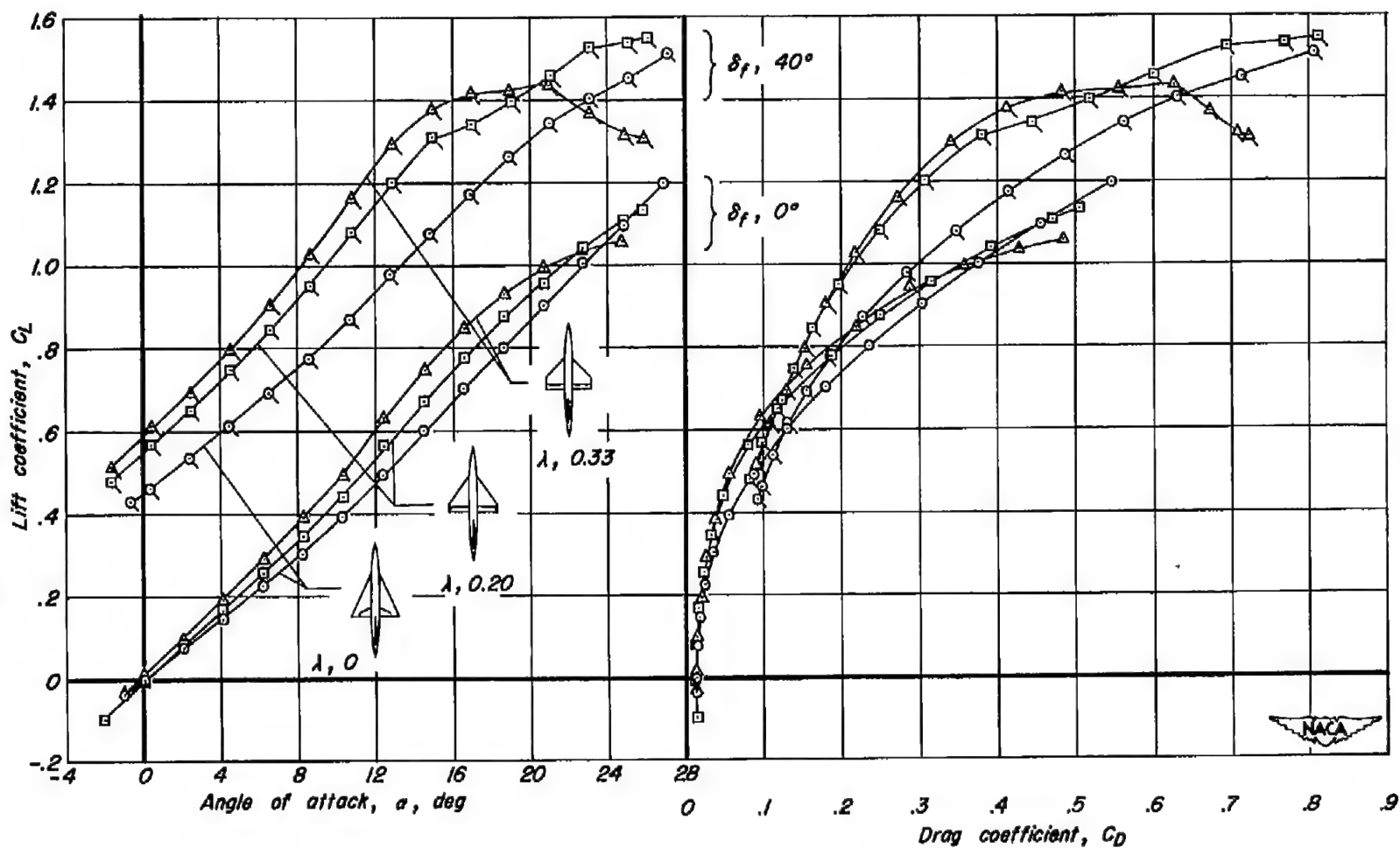
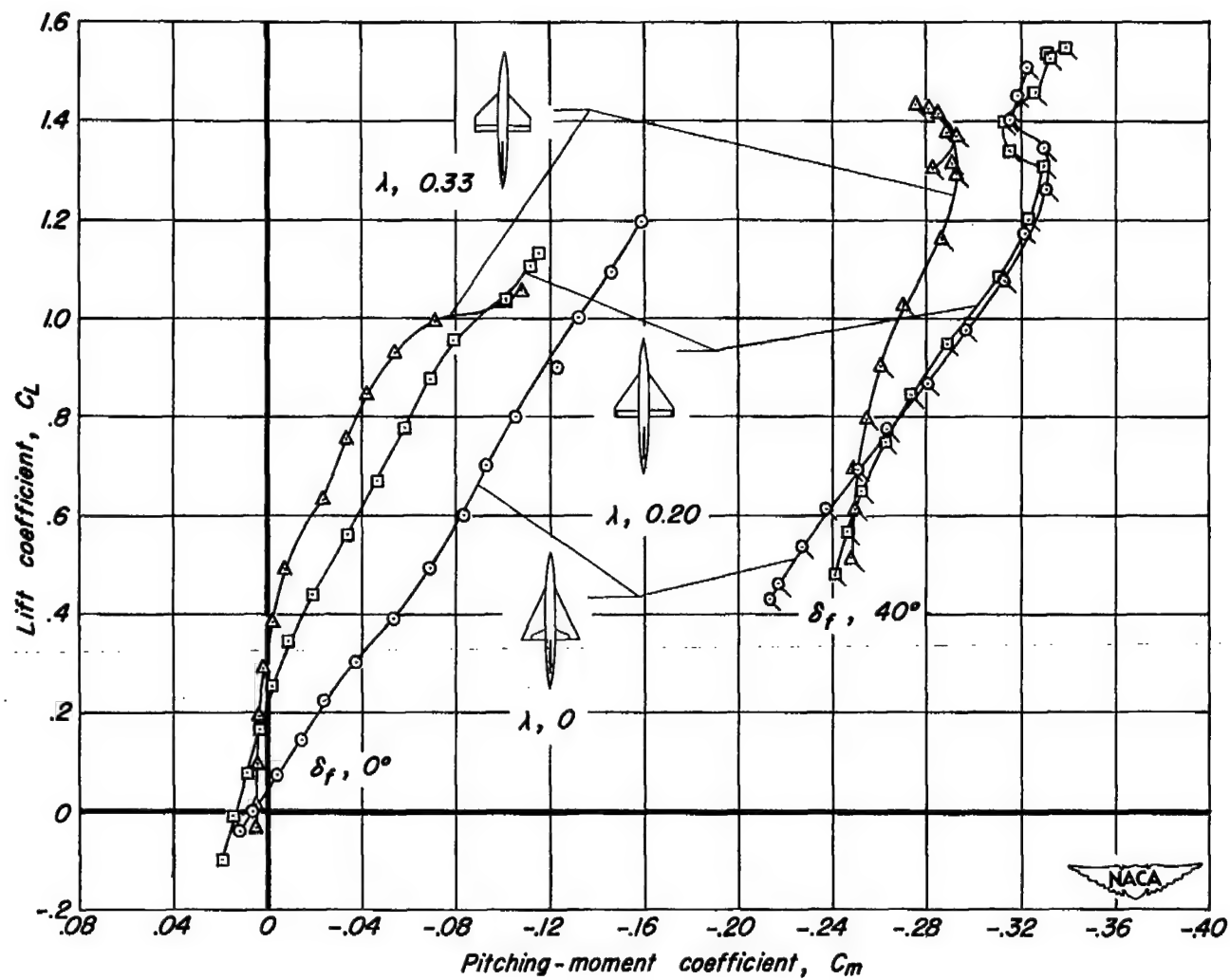
(a)  $C_L$  vs  $\alpha$ ,  $C_D$ 

Figure 4.- Longitudinal characteristics of the three aspect ratio 2 wing models. Horizontal tail off; c.g.,  $0.25\bar{c}$ .



(b)  $C_L$  vs  $C_m$

Figure 4.- Concluded.

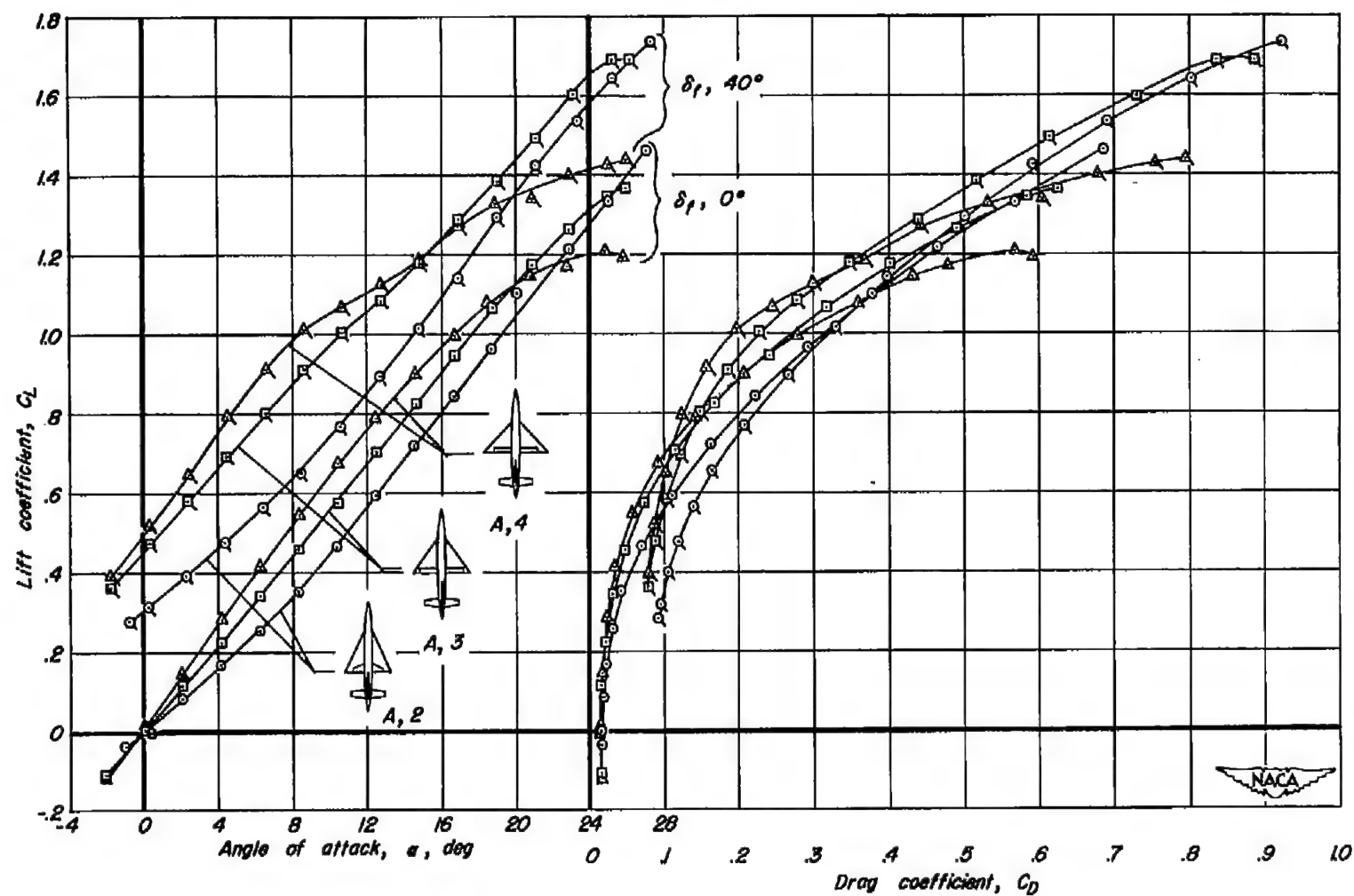
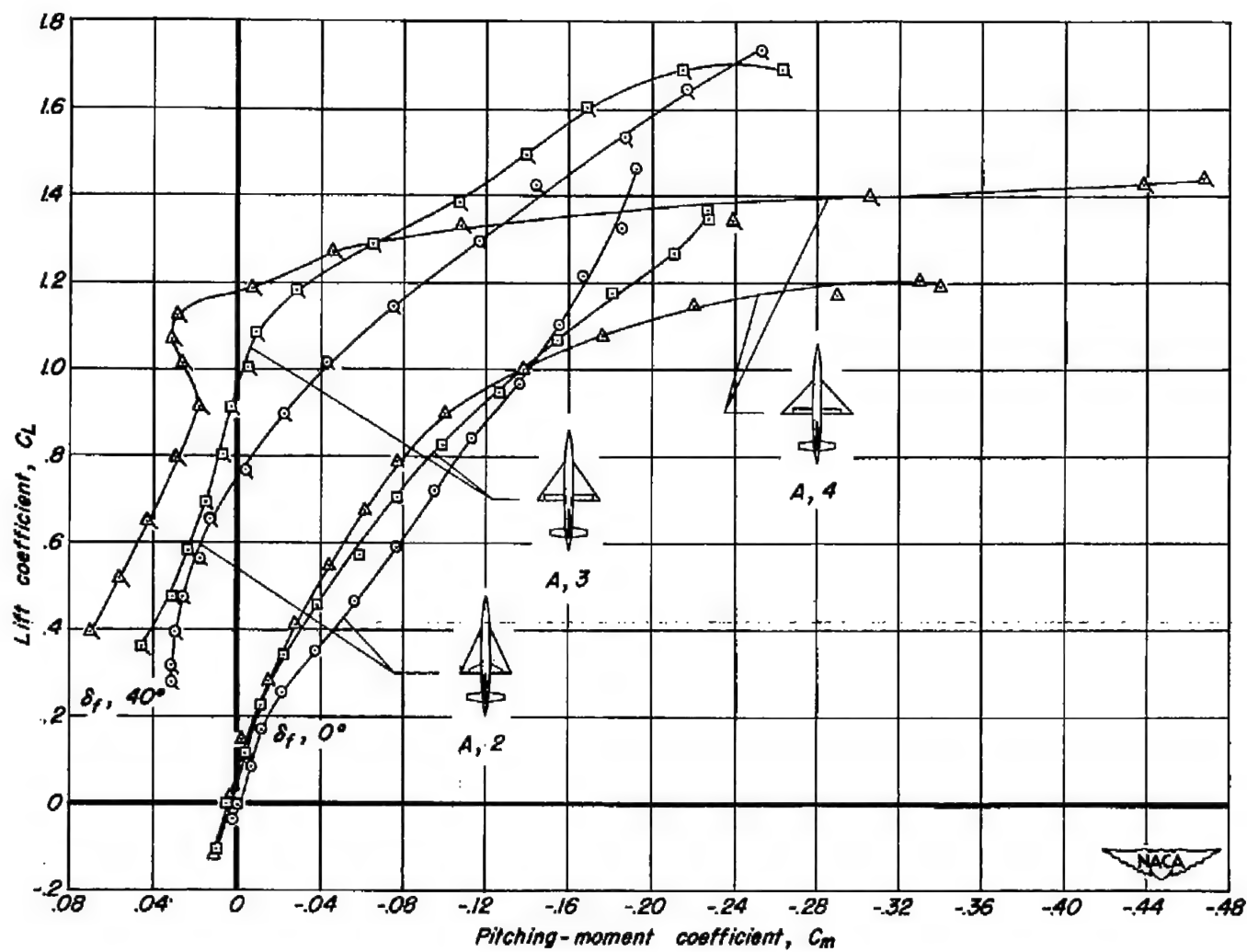
(a)  $C_L$  vs  $\alpha$ ,  $C_D$ 

Figure 5.- Longitudinal characteristics of the three triangular-wing models with the horizontal tails.  $\delta_f, 0^\circ$ ;  $(dC_m/dC_L)_{C_L=0} = 0, -0.06$ .



(b)  $C_L$  vs  $C_m$

Figure 5.- Concluded.

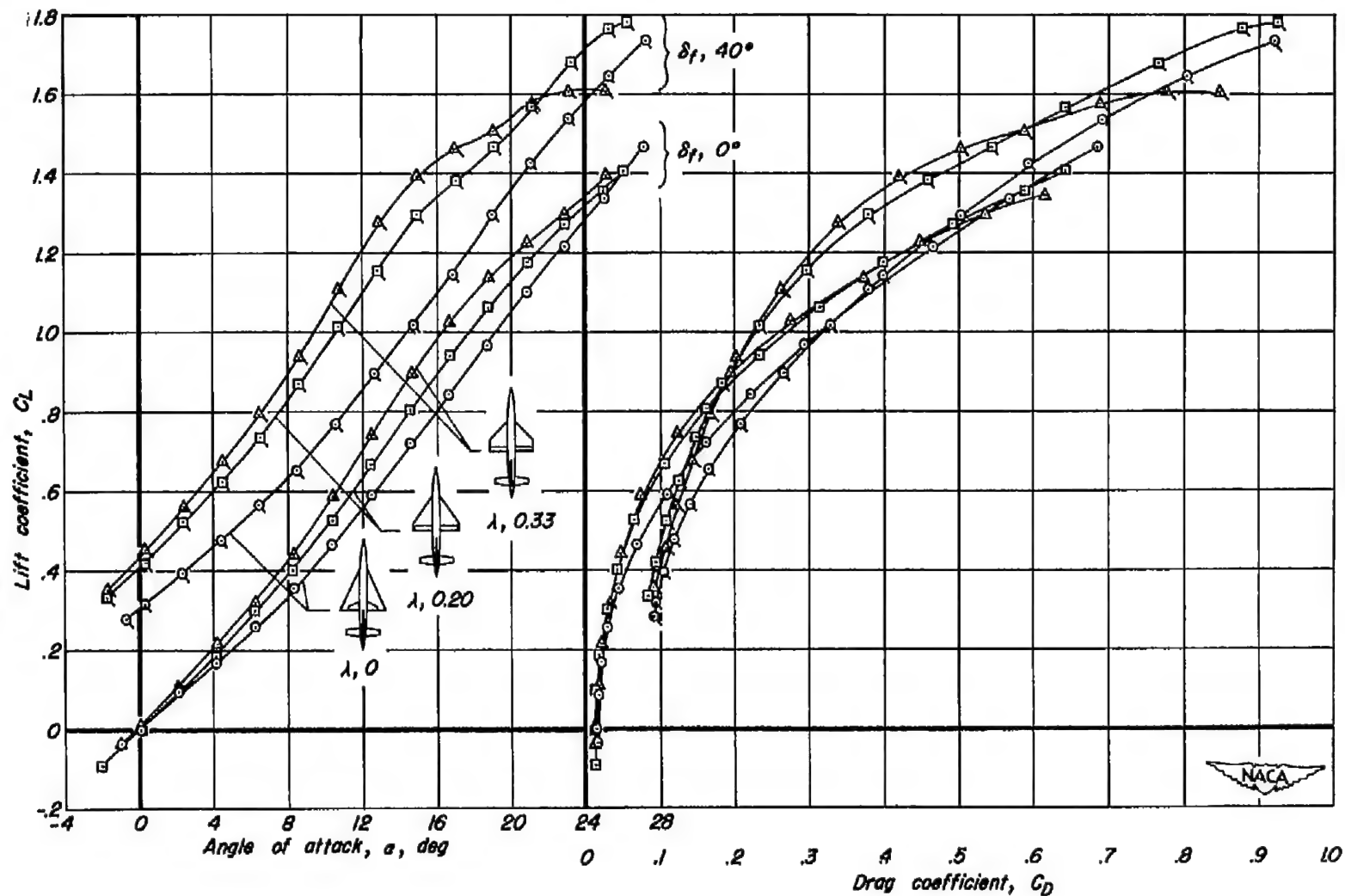
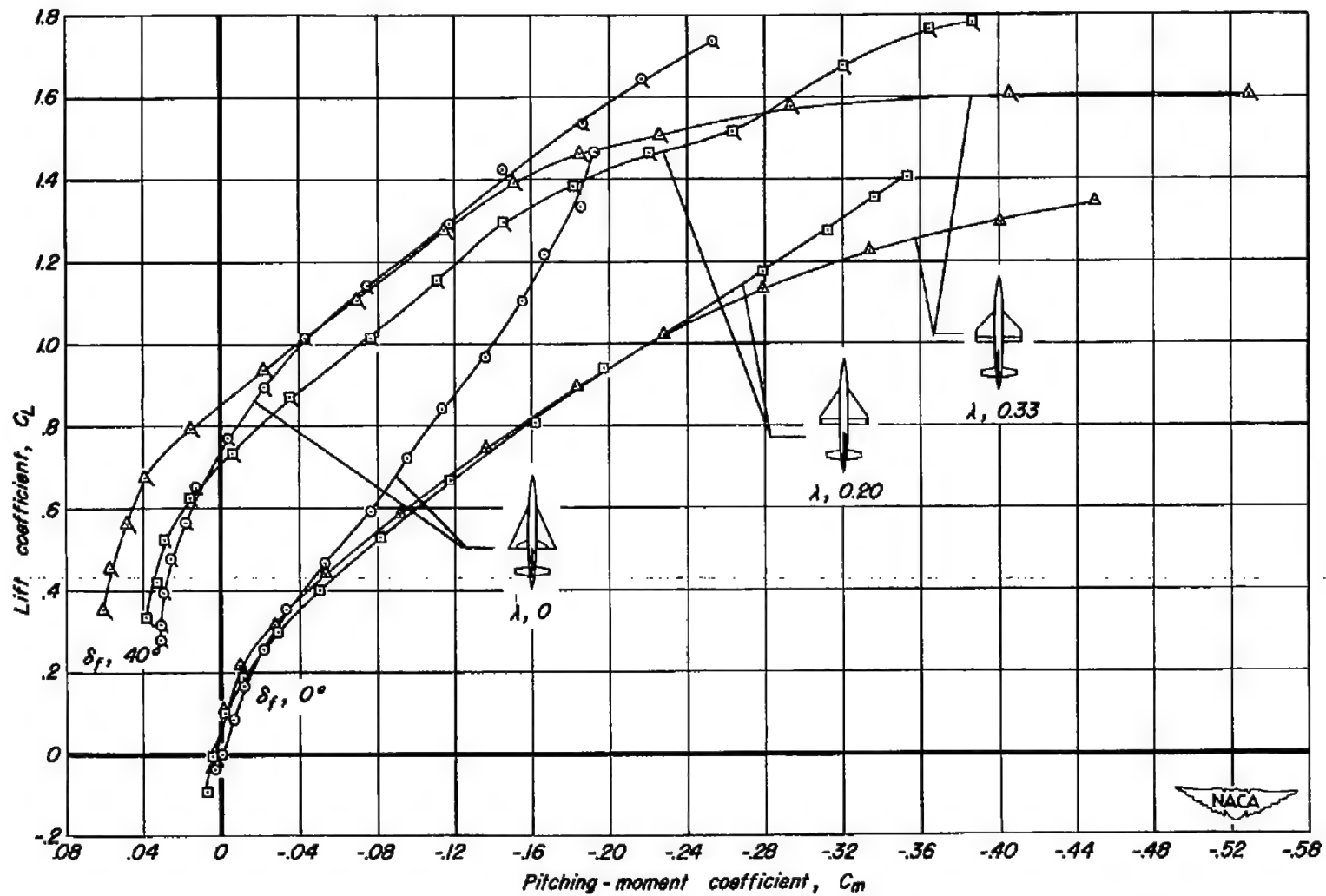
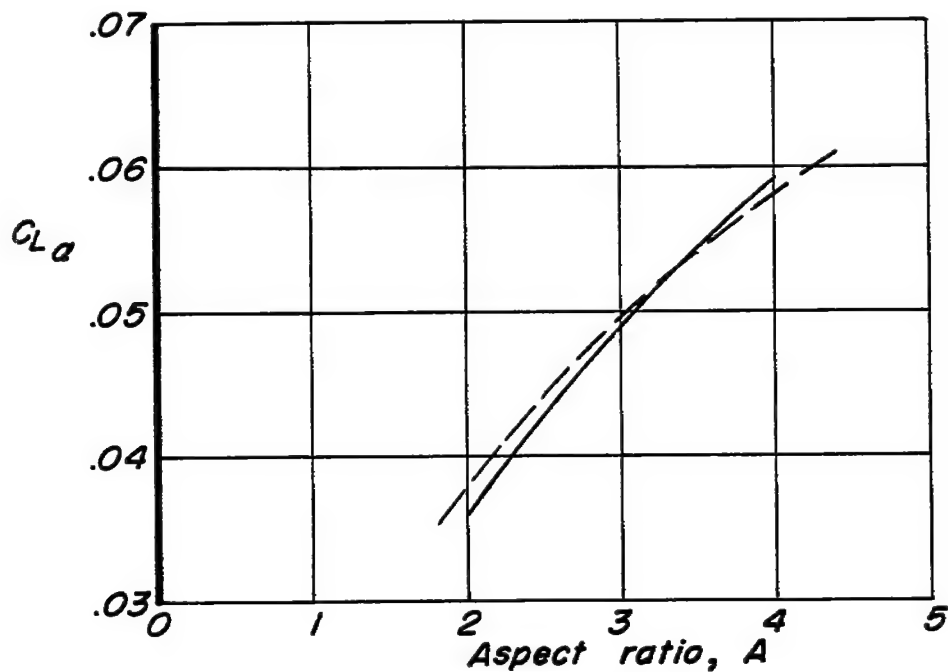
(a)  $C_L$  vs  $\alpha$ ,  $C_D$ 

Figure 6.- Longitudinal characteristics of the three aspect ratio 2 wing models with the horizontal tails.  $\delta_f, 0^\circ$ ;  $(dC_m/dC_L)_{C_L=0} = 0, -0.06$ .

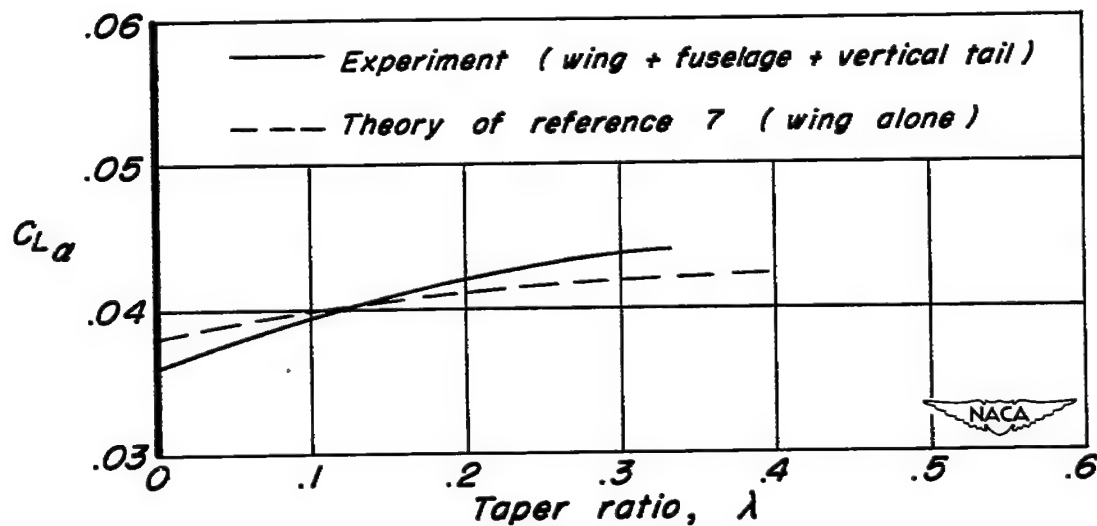


(b)  $C_L$  vs  $C_m$

Figure 6.- Concluded.



(a)  $C_{L\alpha}$  vs  $A$  for triangular wings.



(b)  $C_{L\alpha}$  vs  $\lambda$  for aspect ratio 2 wings.

Figure 7.- Variation of lift-curve slope at  $C_L = 0$  with aspect ratio and taper ratio for the triangular and aspect ratio 2 wings.

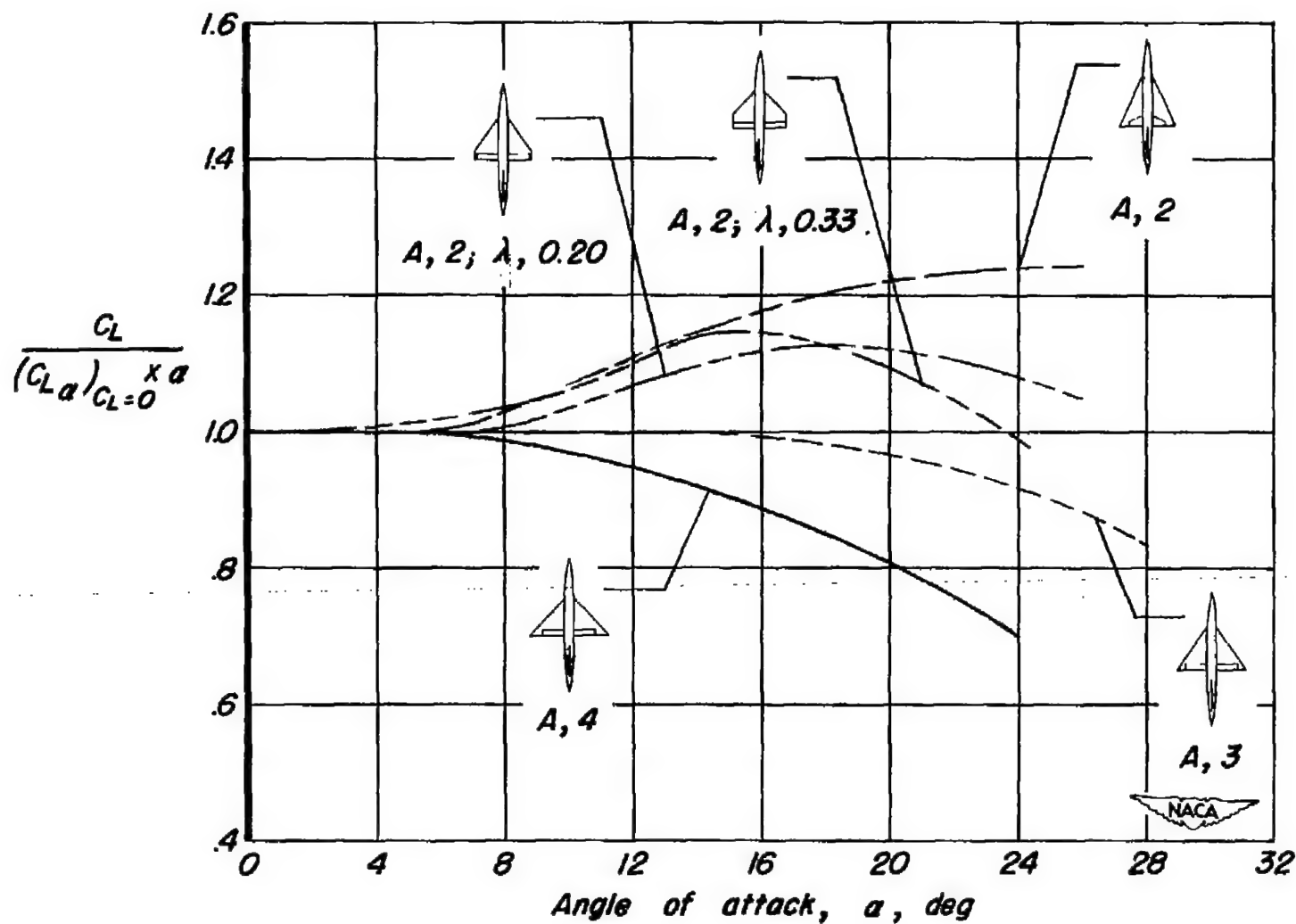


Figure 8.- Variation with angle of attack of the ratio of experimental lift coefficient to lift coefficient obtained by use of lift-curve slope at zero lift.

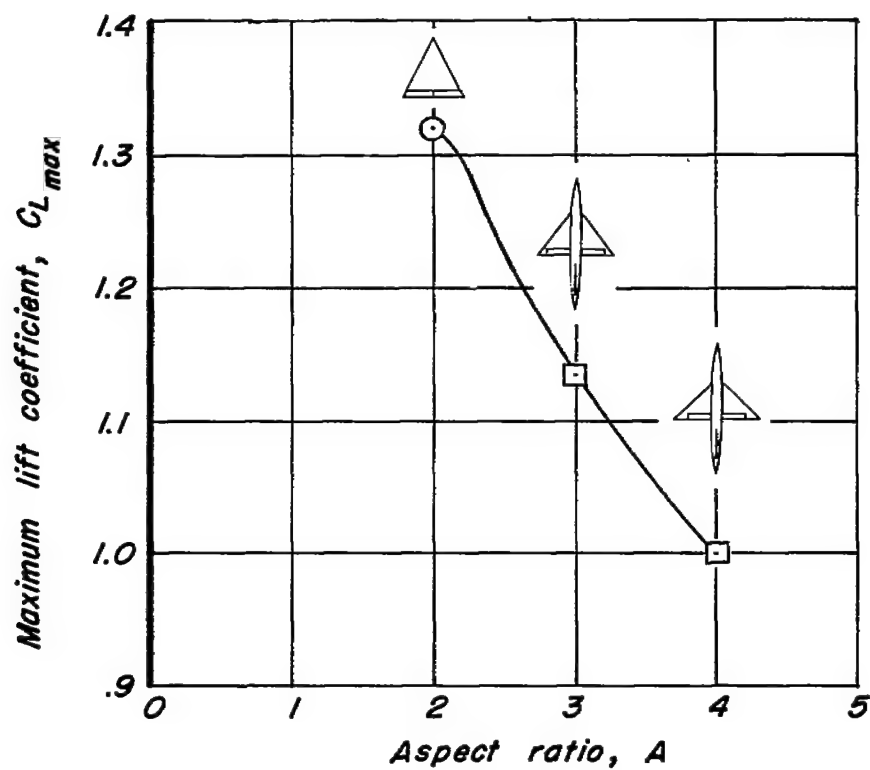
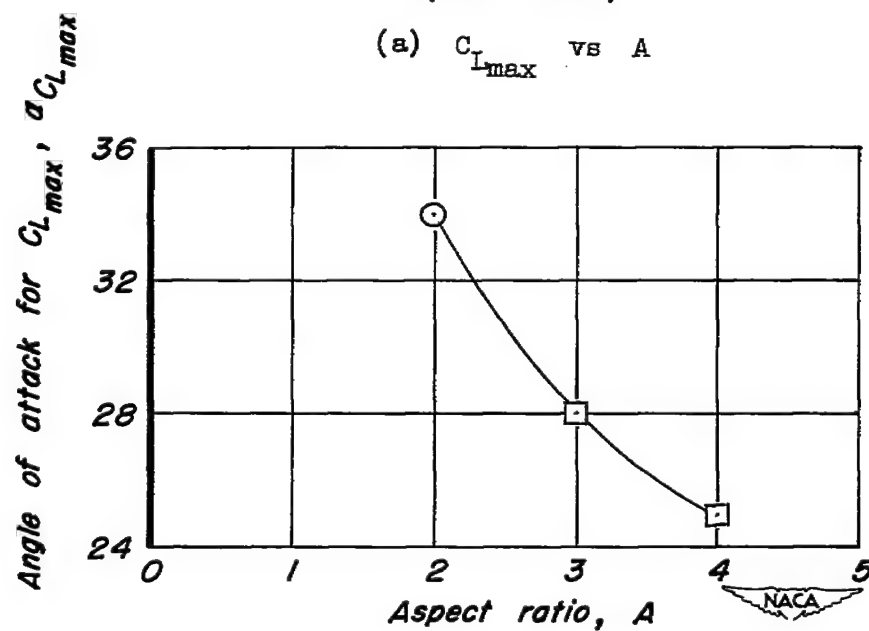
(a)  $C_{L_{max}}$  vs  $A$ (b)  $\alpha_{C_{L_{max}}}$  vs  $A$ 

Figure 9.- Variation with aspect ratio of maximum lift coefficient, and angle of attack for maximum lift coefficient for the triangular-wing models.

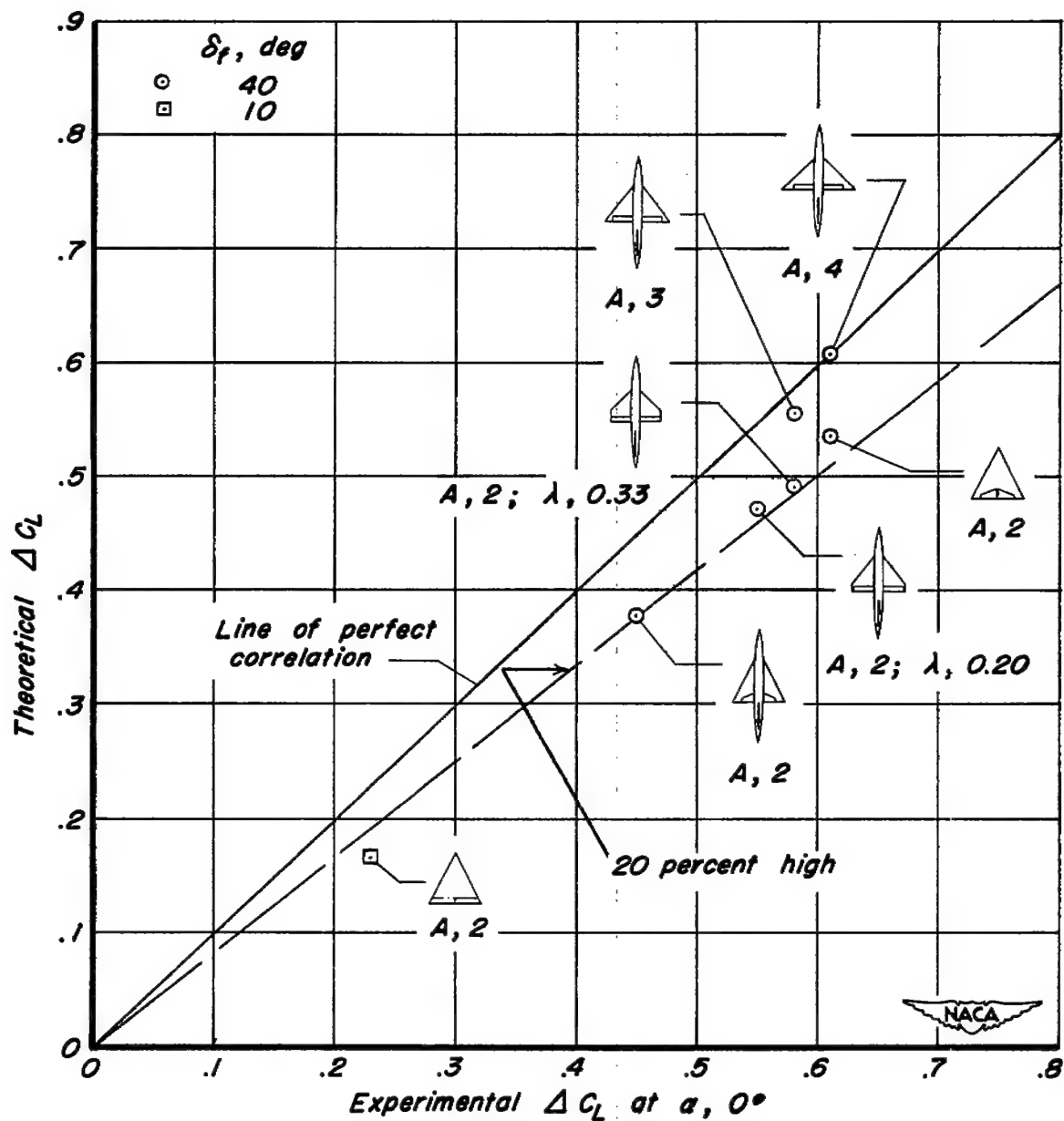


Figure 10.- Comparison of experimental and theoretical increments of lift due to flaps on a series of low aspect ratio wings.

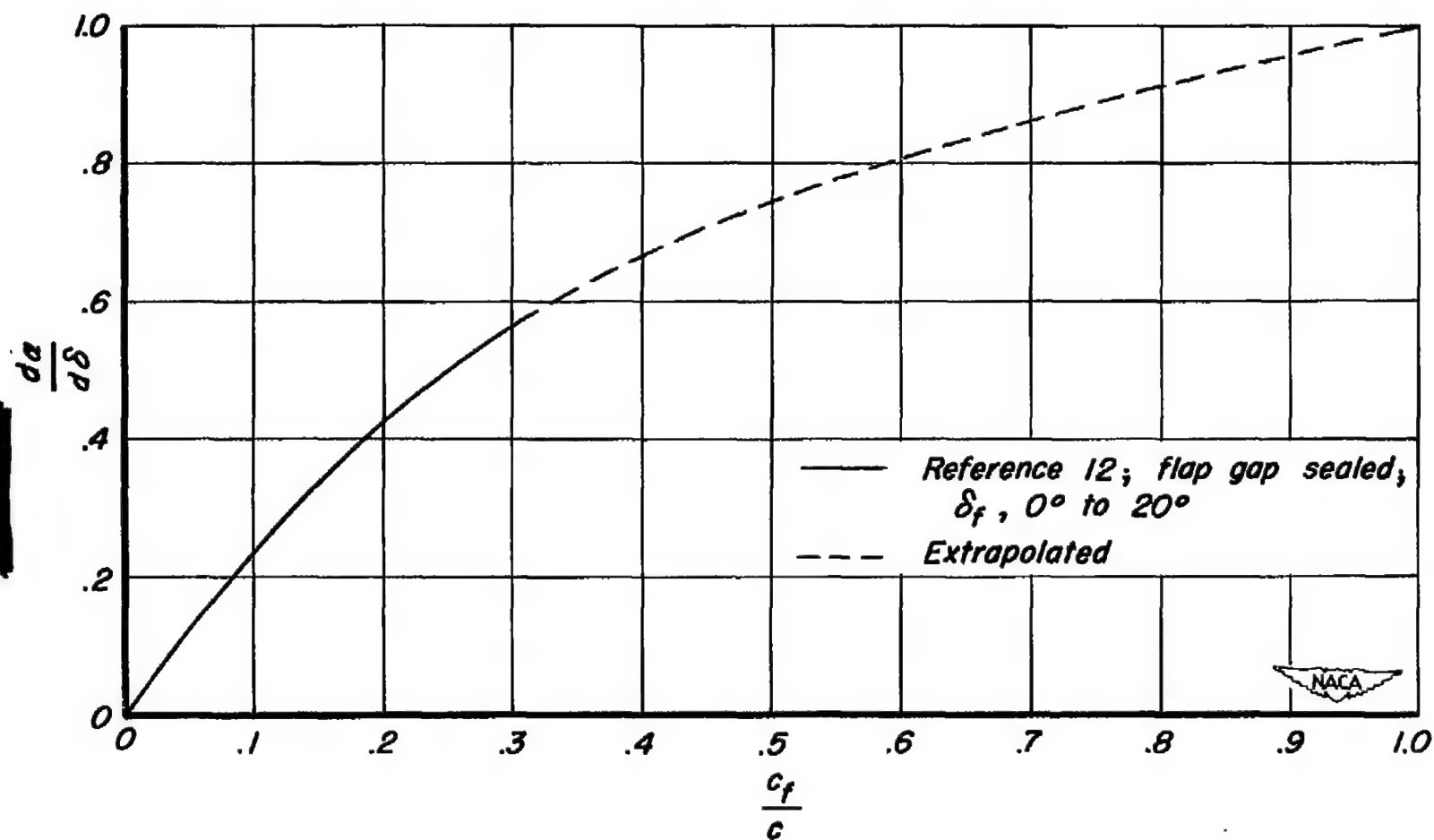


Figure 11.- Variation of  $da/d\delta$  with  $c_f/c$  which was used for the calculation of increments of lift due to flaps.

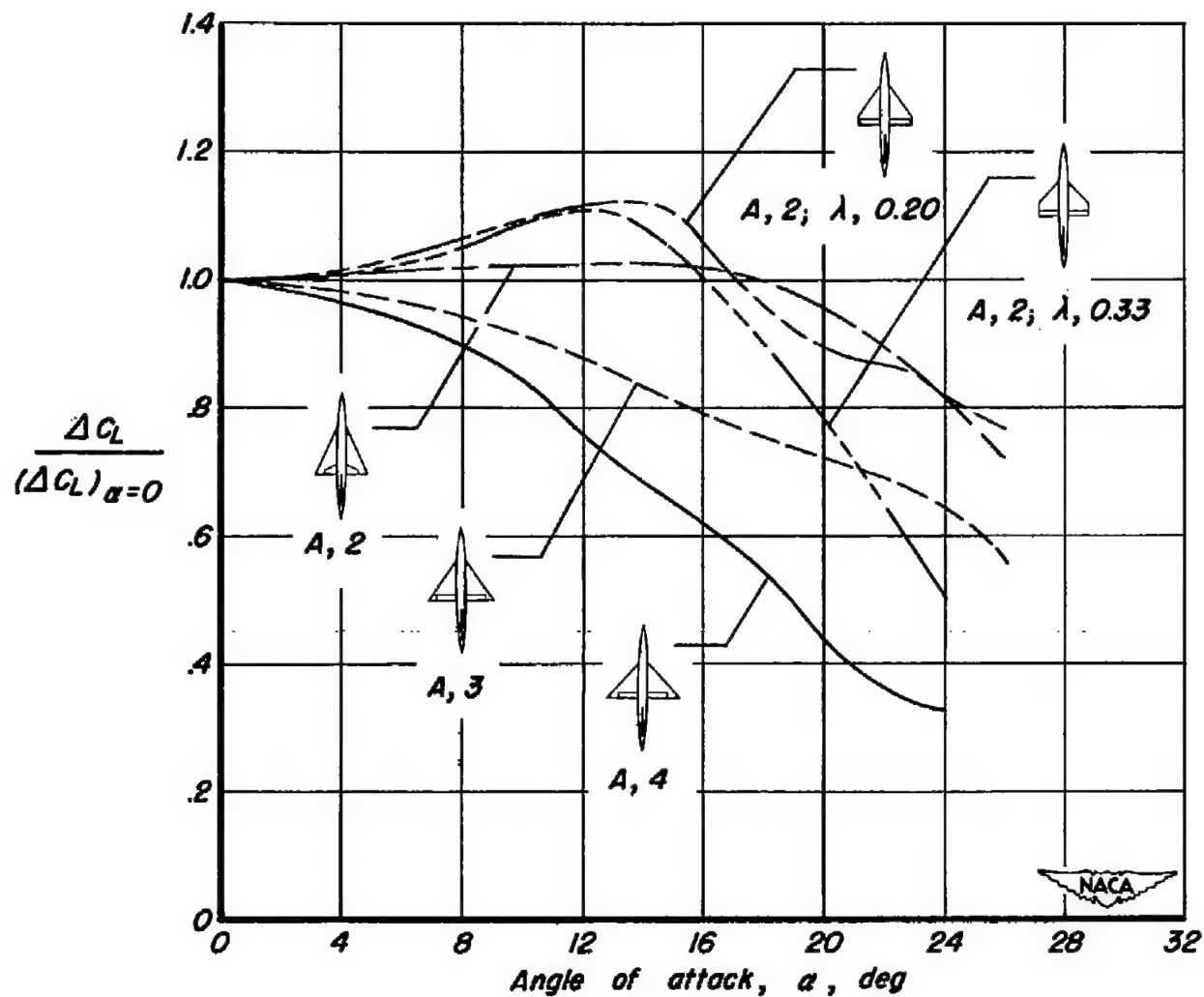
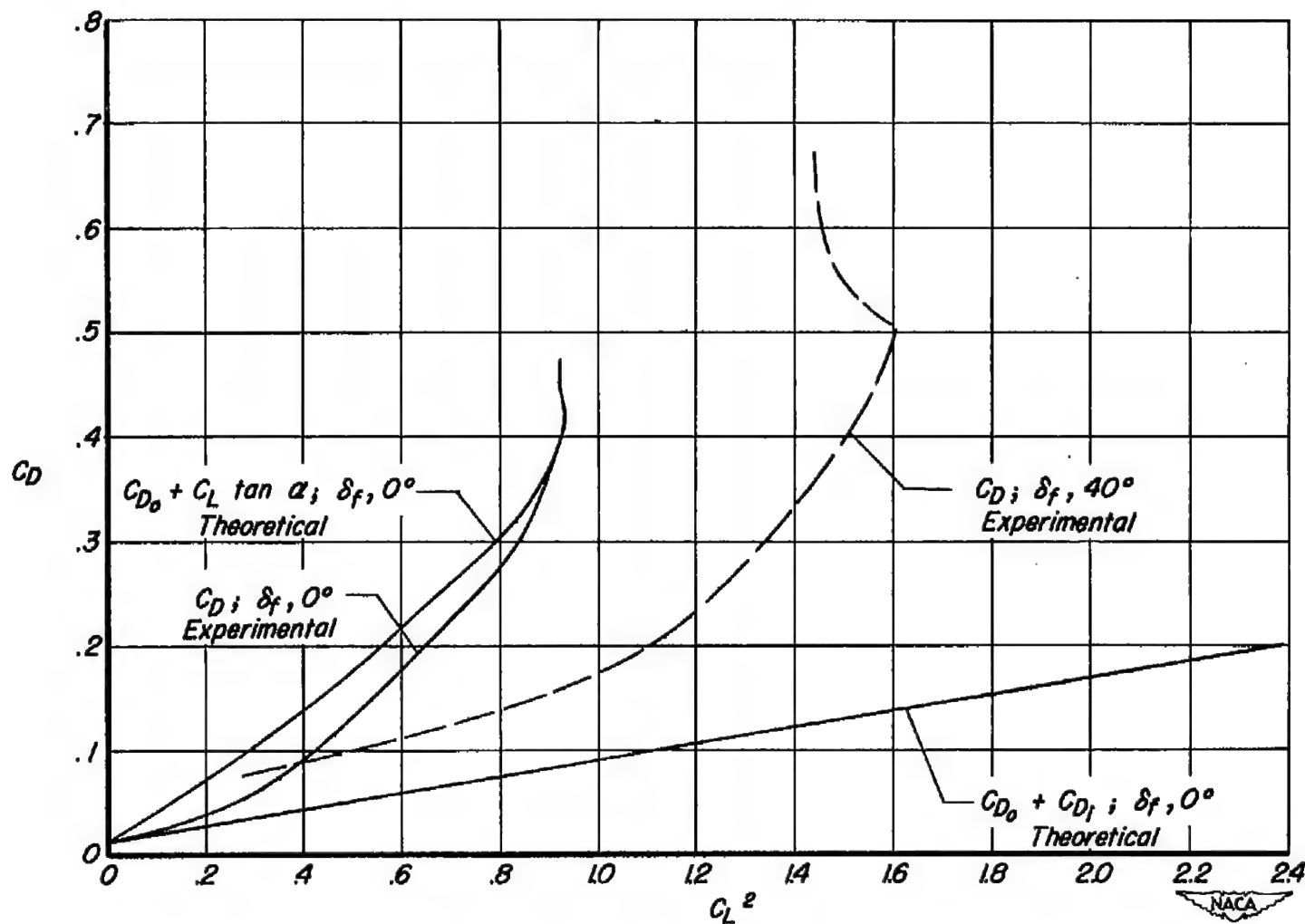
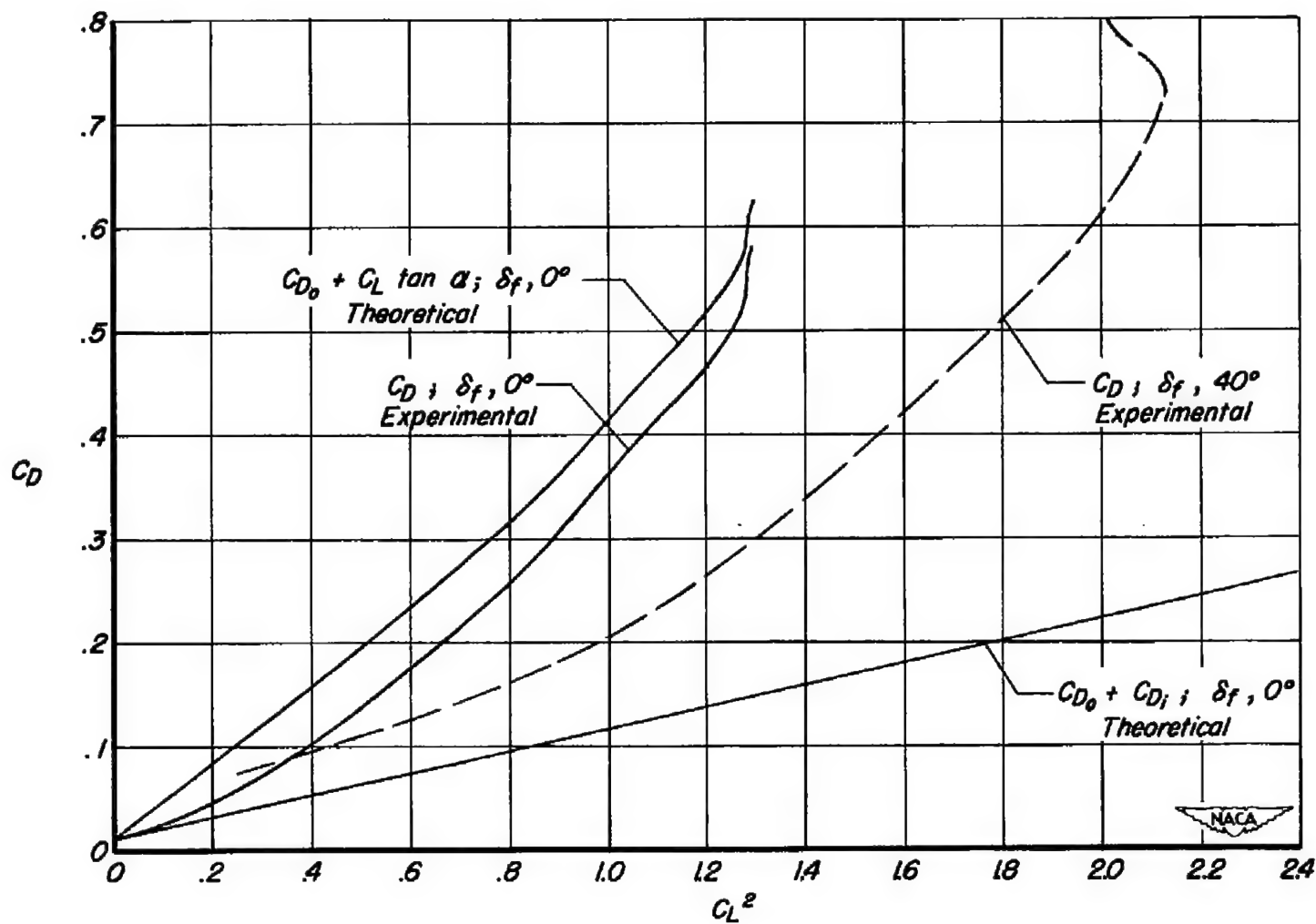


Figure 12.- Variation with angle of attack of the ratio of increment of lift due to flap deflection with the increment of lift at zero angle of attack.  $\delta_f, 40^\circ$ .



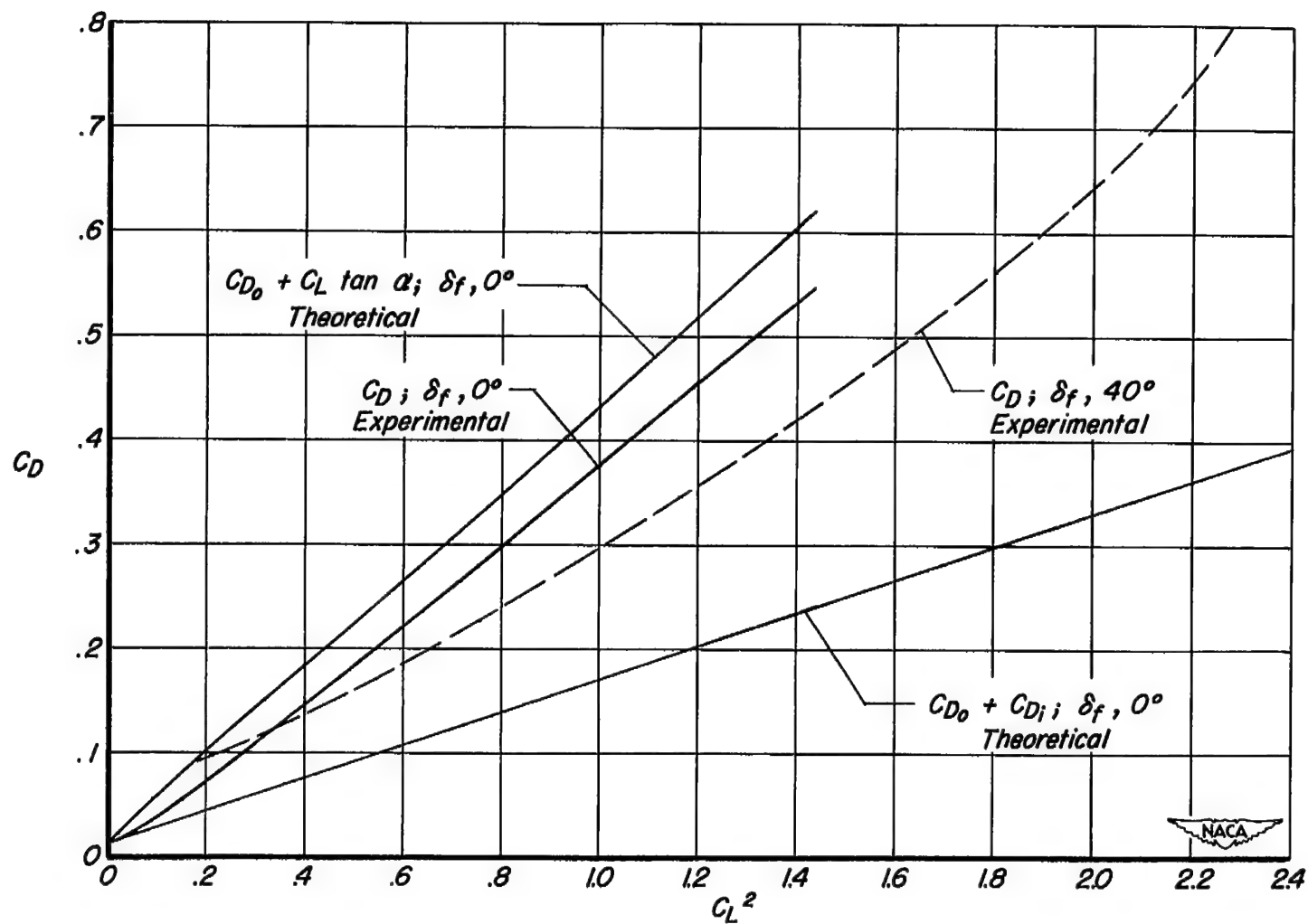
(a) Aspect ratio 4, triangular wing.

Figure 13.- Comparison of experimental and computed drag as a function of lift coefficient squared for the wing-fuselage models.



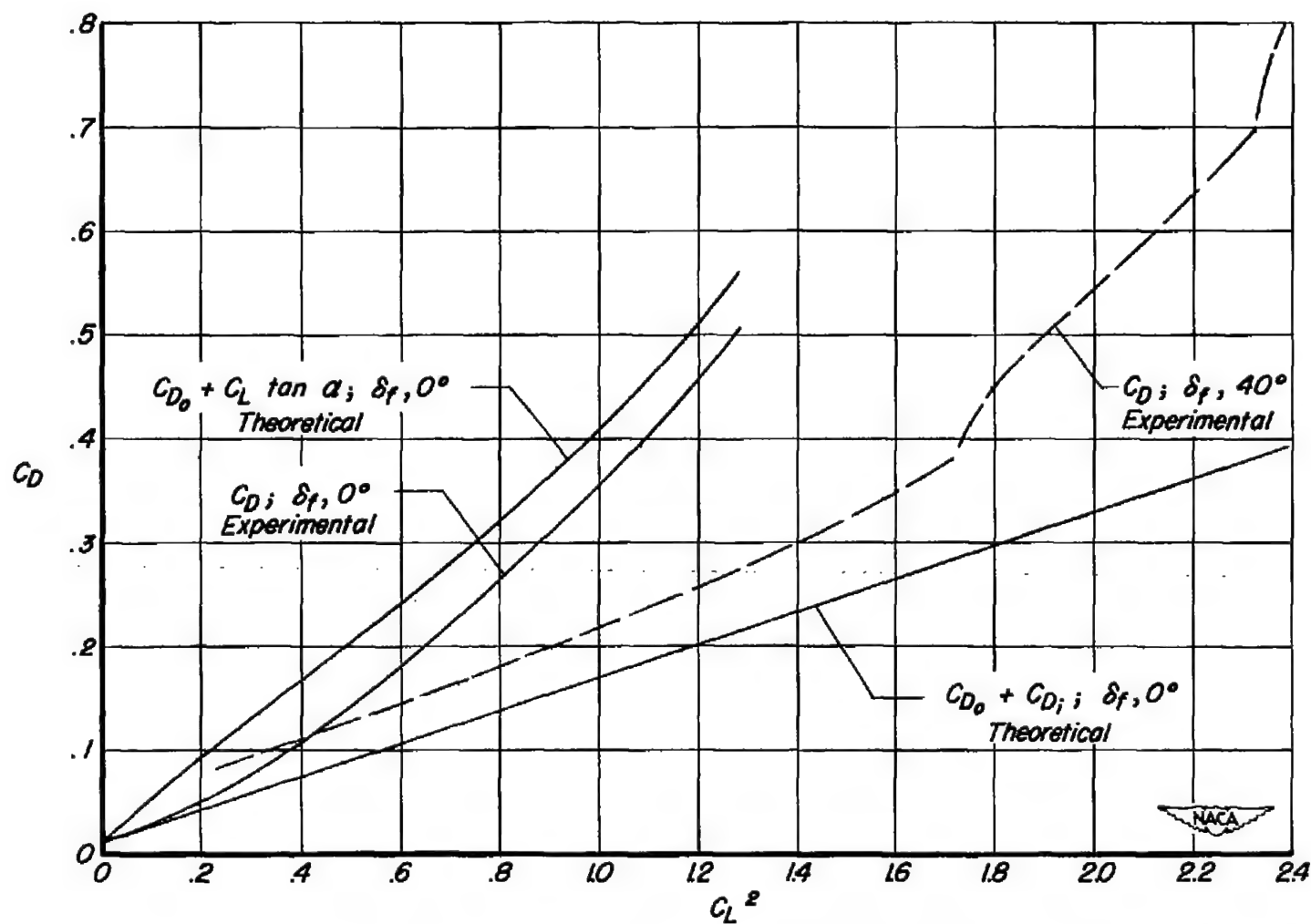
(b) Aspect ratio 3, triangular wing.

Figure 13.- Continued.



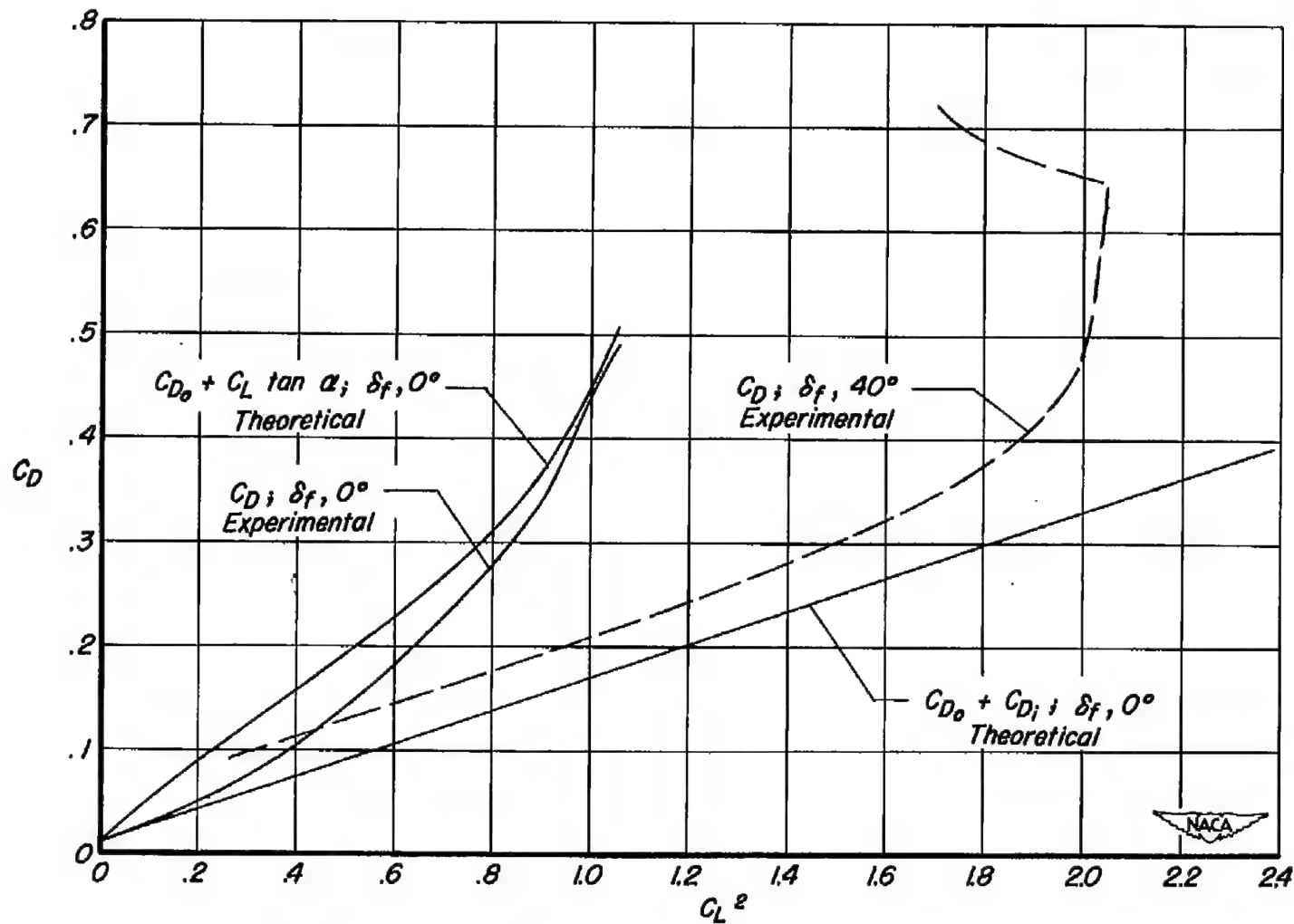
(c) Aspect ratio 2, triangular wing.

Figure 13.- Continued.



(d) Aspect ratio 2, taper ratio 0.20, modified triangular wing.

Figure 13.- Continued.



(e) Aspect ratio 2, taper ratio 0.33, modified triangular wing.

Figure 13.- Concluded.

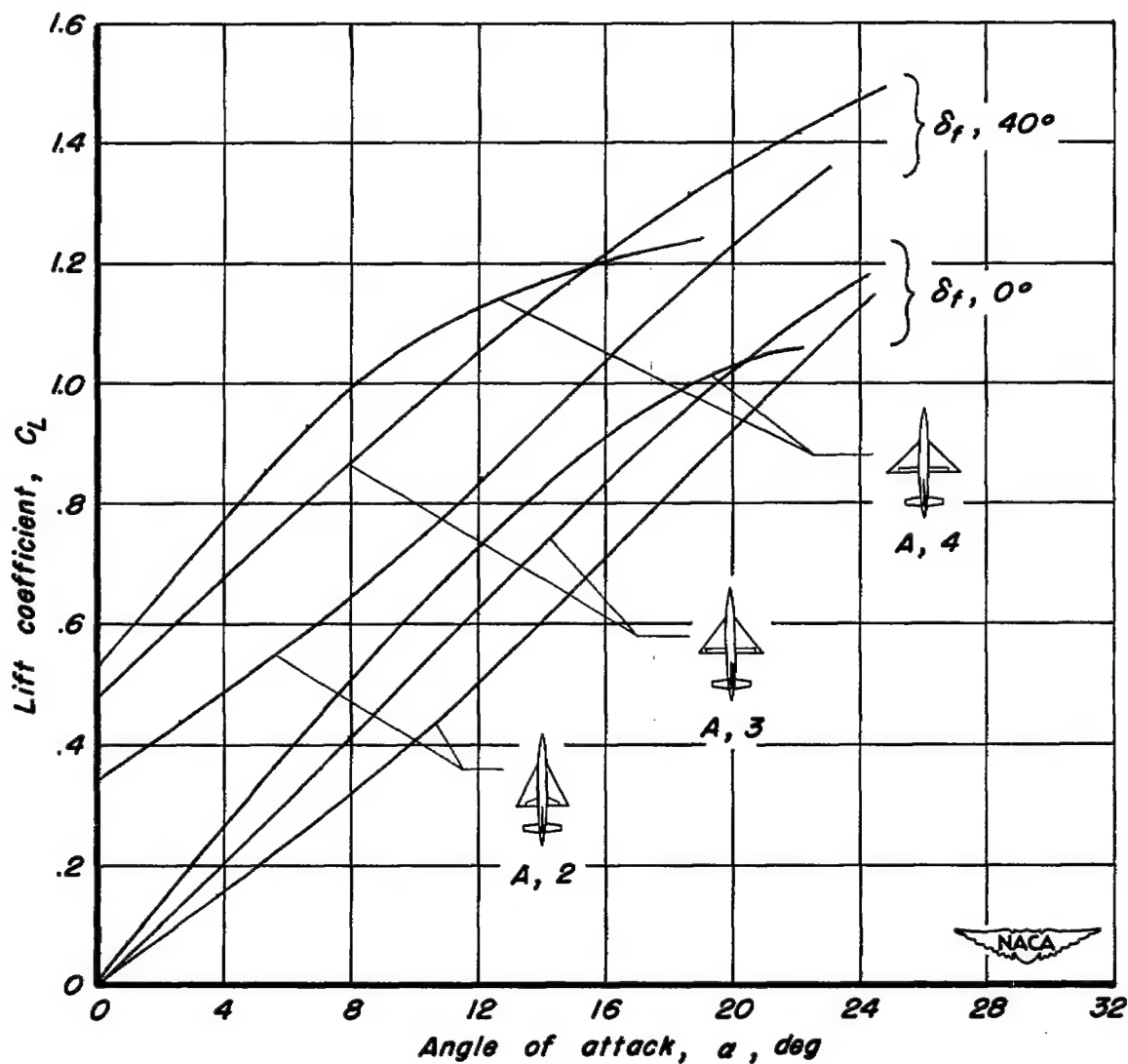


Figure 14.- Lift characteristics of three trimmed triangular-wing airplane models.  $(dC_m/dC_L)_{C_L=0} = 0, -0.06$ .

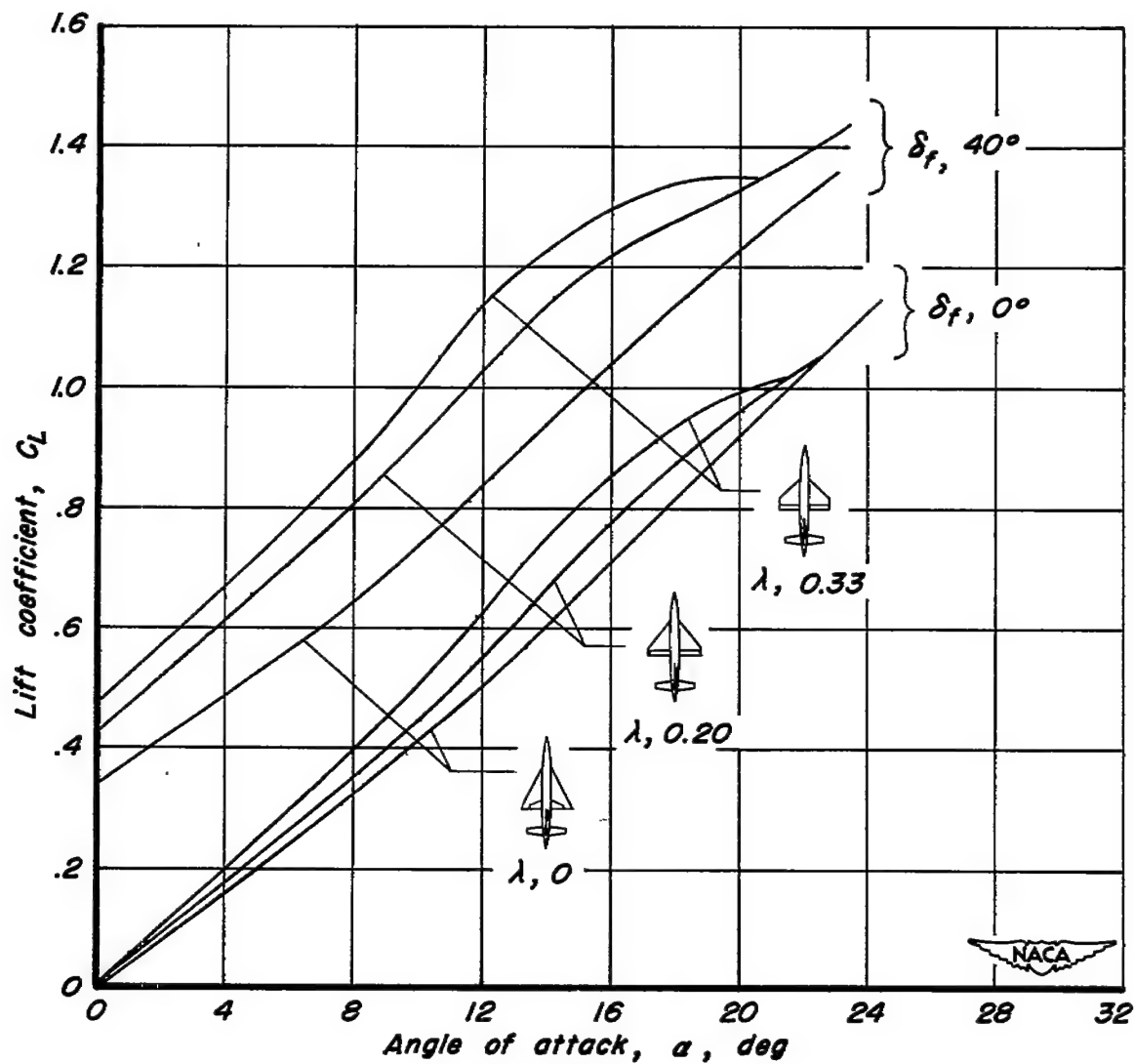


Figure 15.- Lift characteristics of three trimmed aspect ratio 2 wing airplane models.  $(dC_m/dC_L)_{C_L} = 0, -0.06$ .

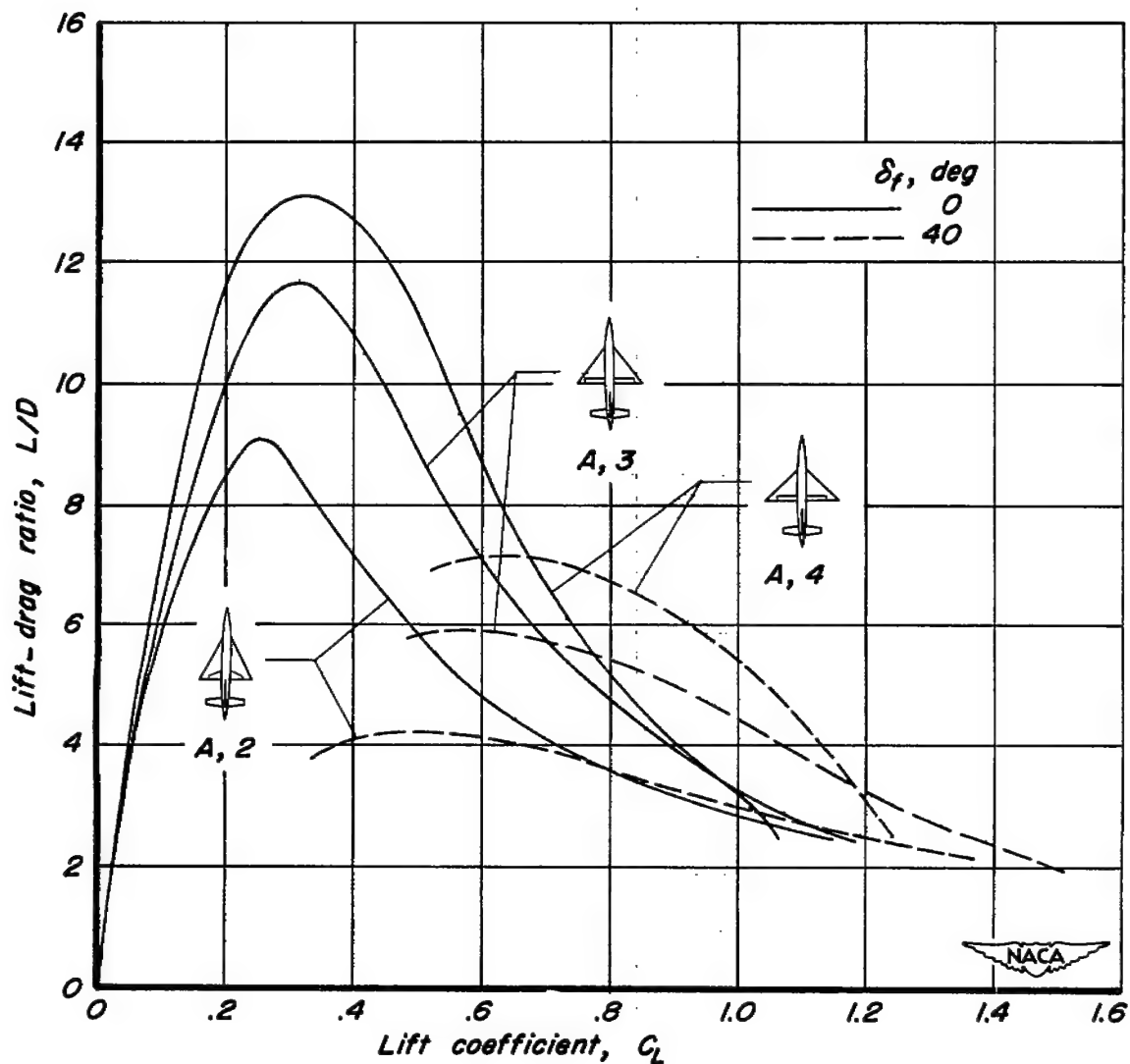


Figure 16.- Variation of lift-drag ratios with lift coefficient of three trimmed triangular-wing airplane models.  $(dC_m/dC_L)_{C_L} = 0, -0.06$ .

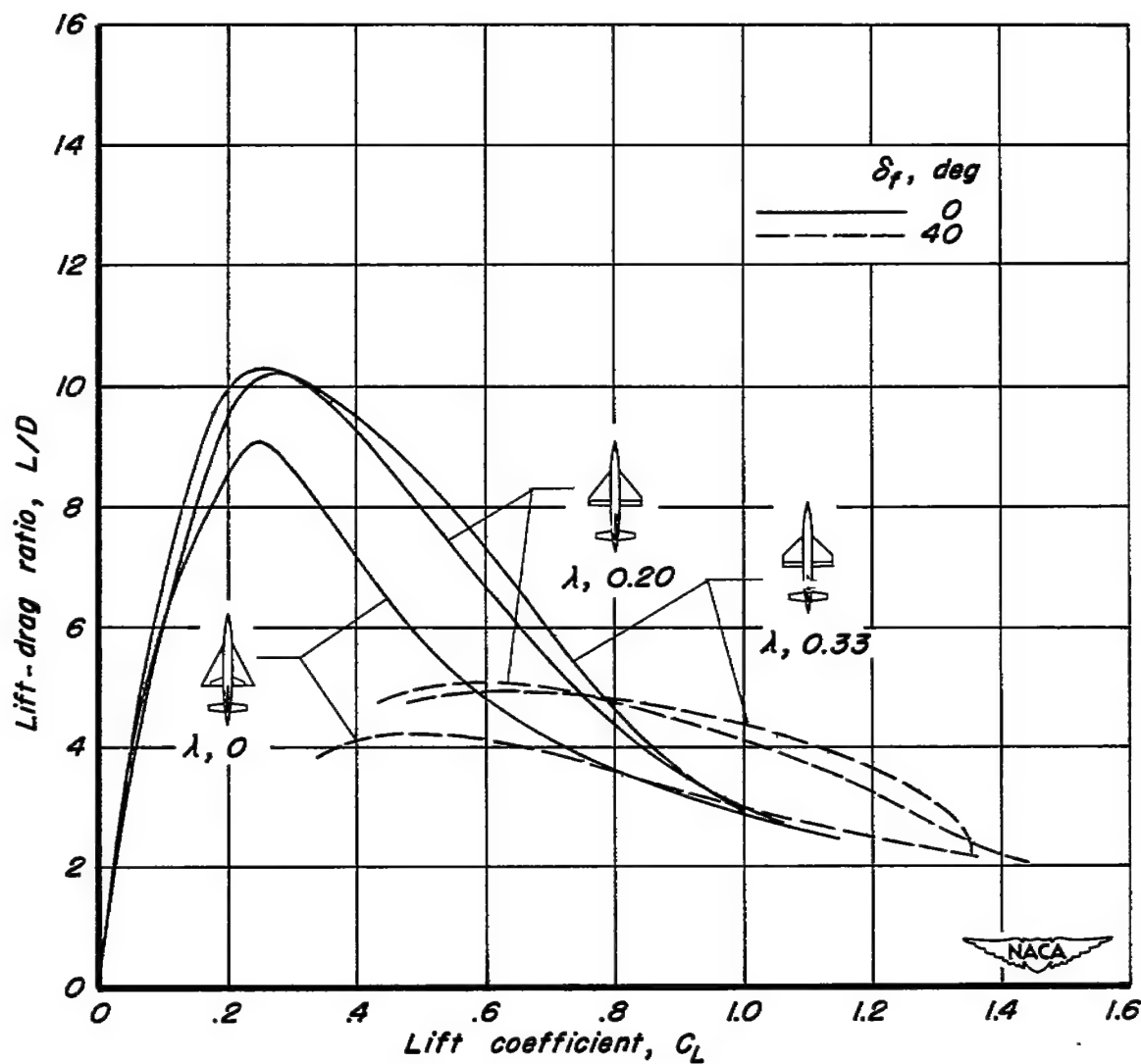


Figure 17.- Variation of lift-drag ratios with lift coefficient of three trimmed aspect ratio 2 wing airplane models.  $(dC_m/dC_L)_{C_L} = 0, -0.06$ .

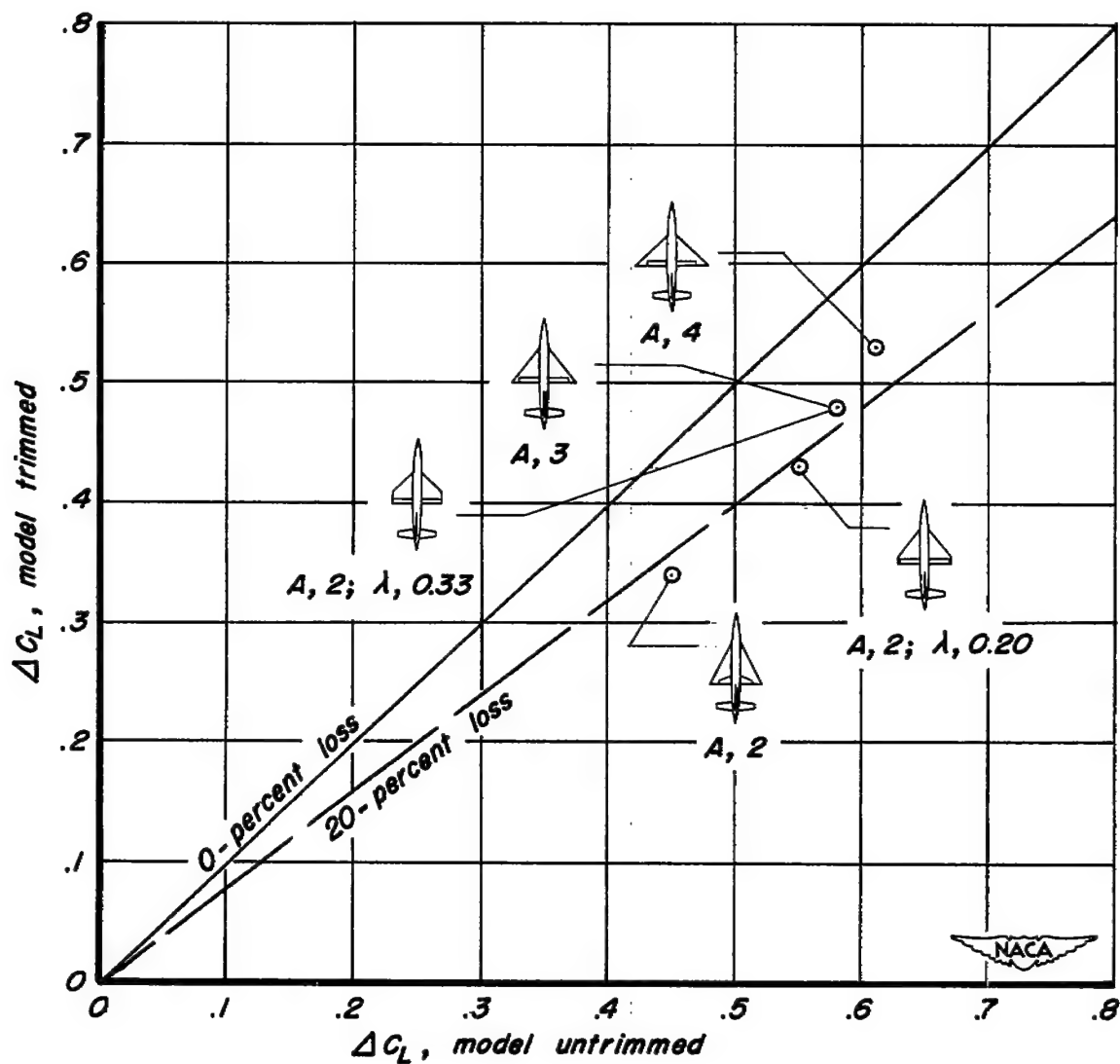


Figure 18.- Effect of trimming the models for a 6-percent static margin on the increment of lift due to flaps.  $\alpha$ ,  $0^\circ$ ;  $\Delta\delta_f$ ,  $40^\circ$ .

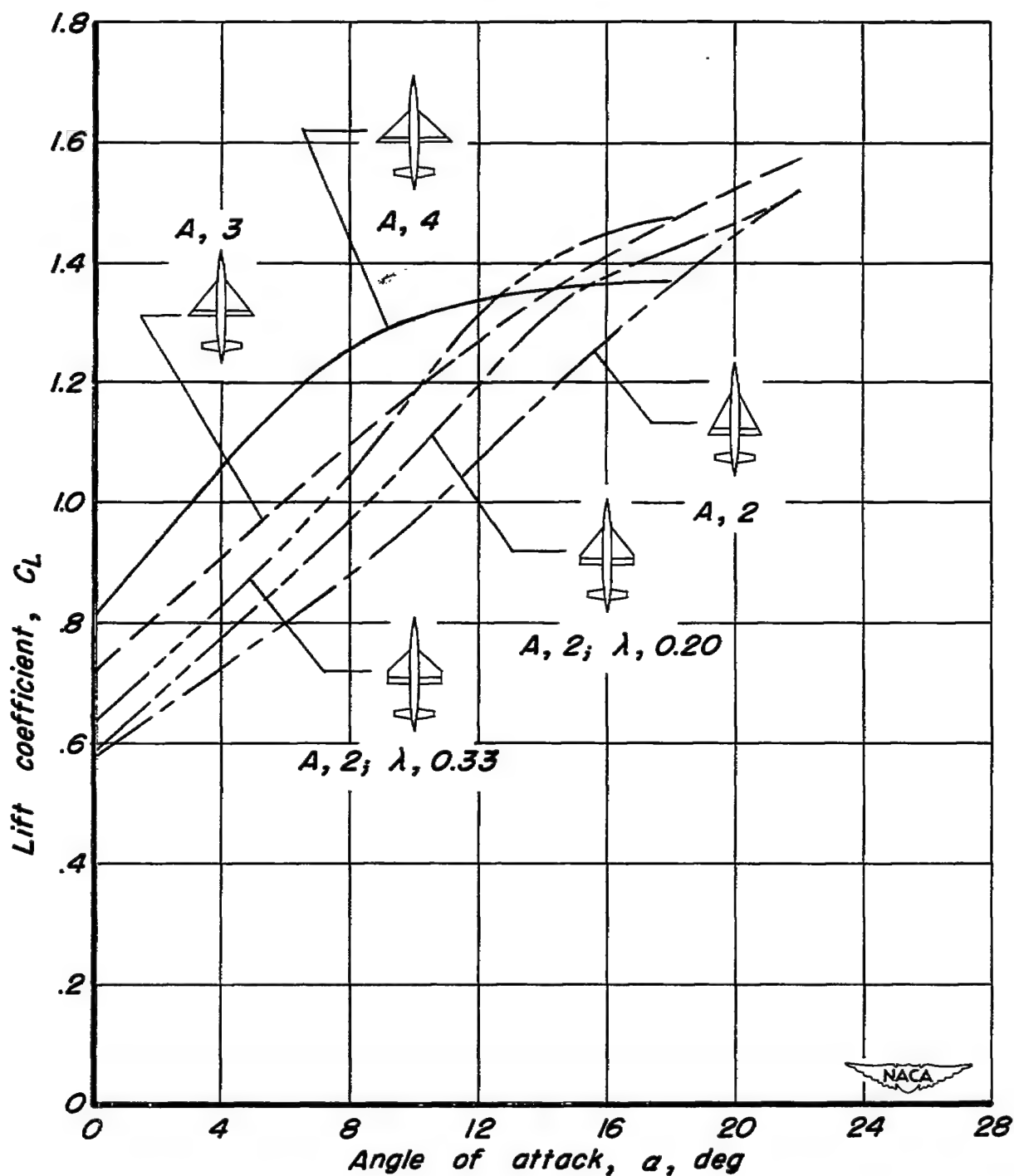


Figure 19.- Comparison of the computed lift characteristics of five trimmed airplane models having 20-percent wing area, full-span, constant-chord flaps.  $\delta_f, 40^\circ$ ;  $(dC_m/dC_L)_{C_L=0} = 0, -0.06$ .

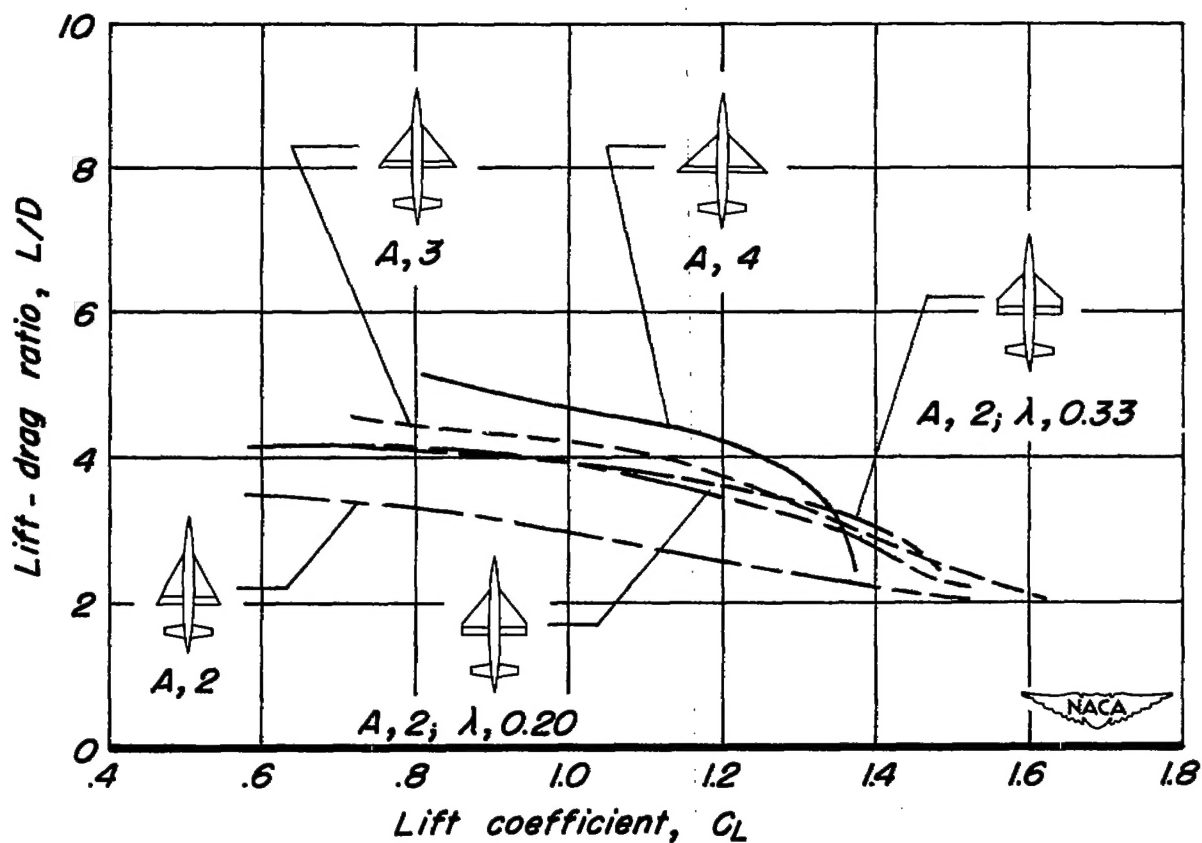


Figure 20.- Comparison of the computed lift-drag ratios of the landing configurations of five trimmed airplane models having 20-percent wing area, full-span, constant-chord flaps. Gear down;  $\delta_f, 40^\circ$ ;  $(dC_m/dC_L)_{C_L} = 0, -0.06$ .

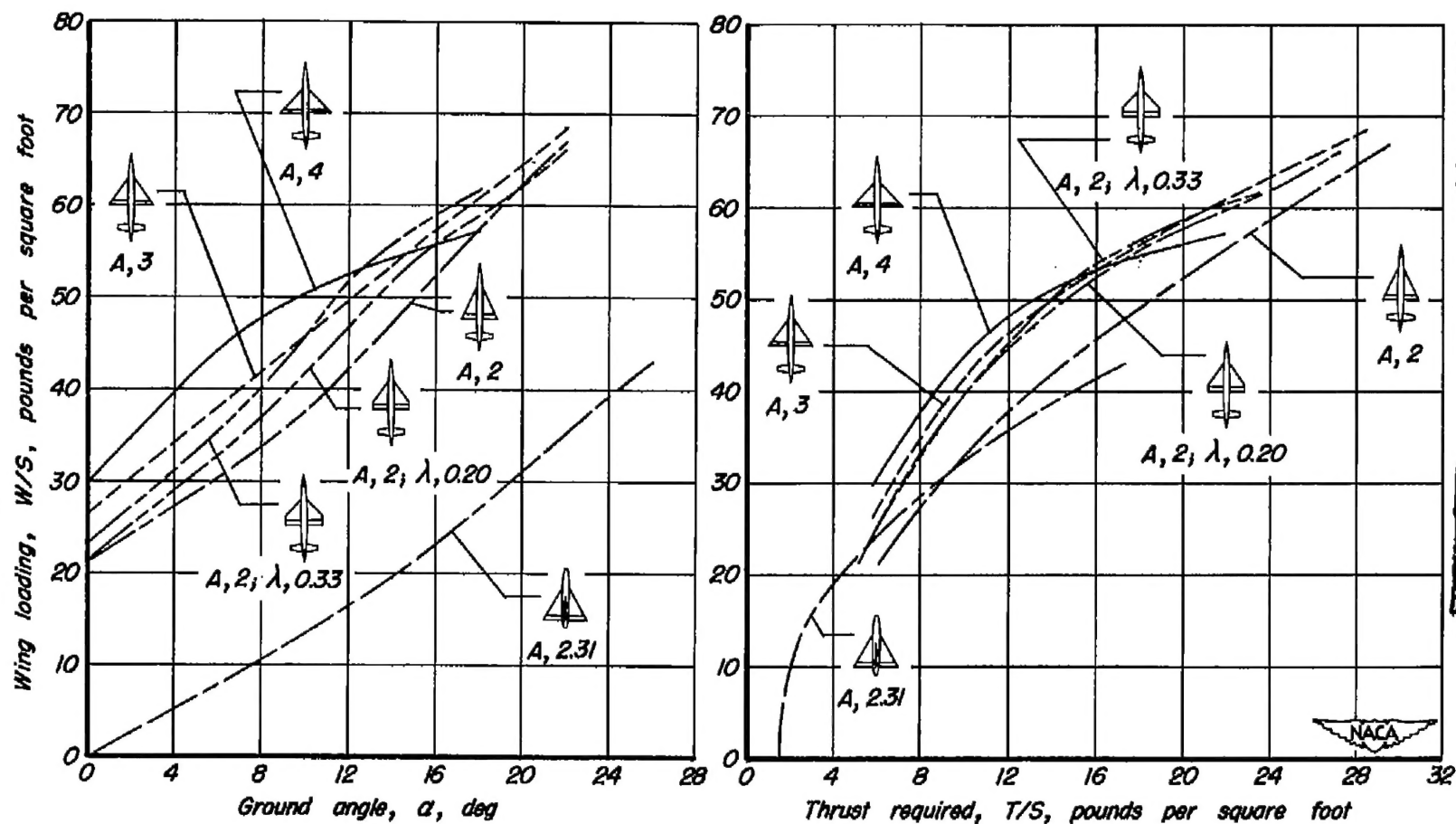


Figure 21.- Maximum wing loadings and thrusts required for six airplane models at a horizontal speed of 120 miles per hour and zero sinking speeds. Gear down;  $\delta_F$ ,  $40^\circ$  for models with horizontal tails;  $(dC_m/dC_L)_{C_L} = 0$ ,  $-0.06$ .

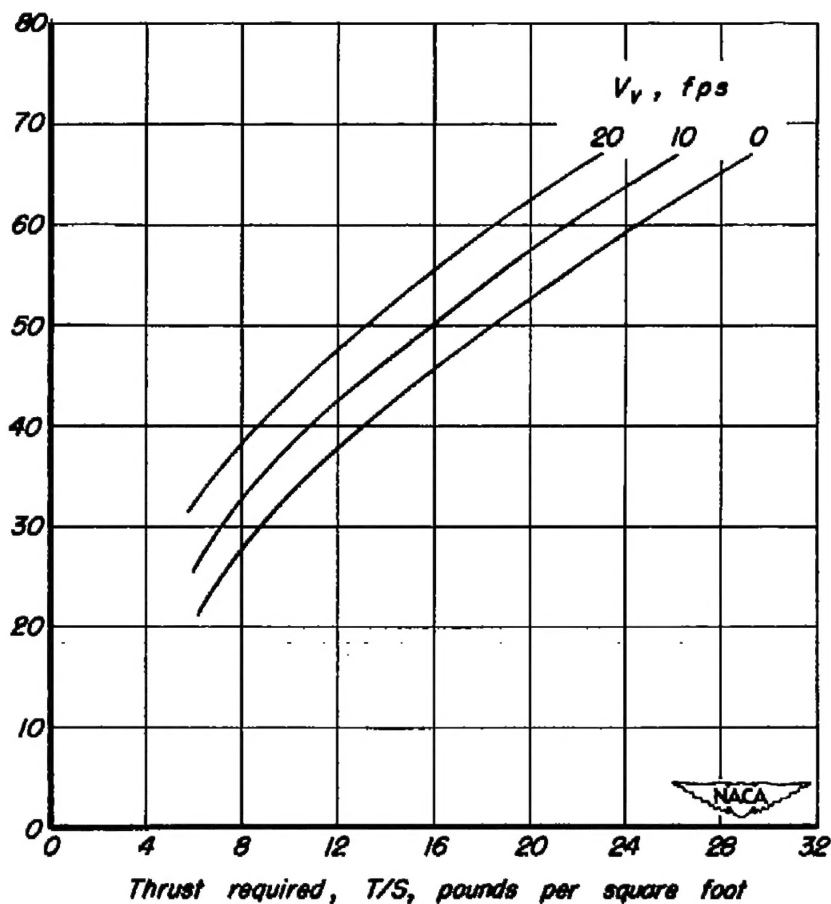
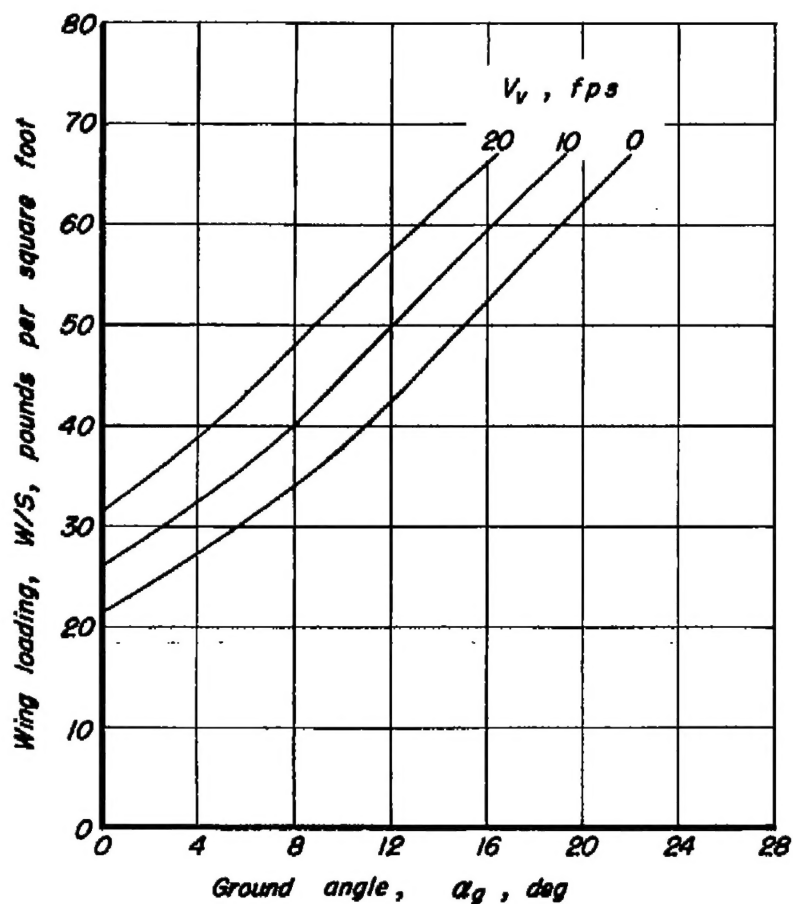


Figure 22.- Effect of assumed sinking speeds on the maximum wing loadings and thrusts required for the aspect ratio 2, triangular wing model at a horizontal speed of 120 miles per hour. Gear down;  $\delta_f$ ,  $40^\circ$ ;  $(\frac{dC_m}{dC_L})_{C_L=0}$ , -0.06.

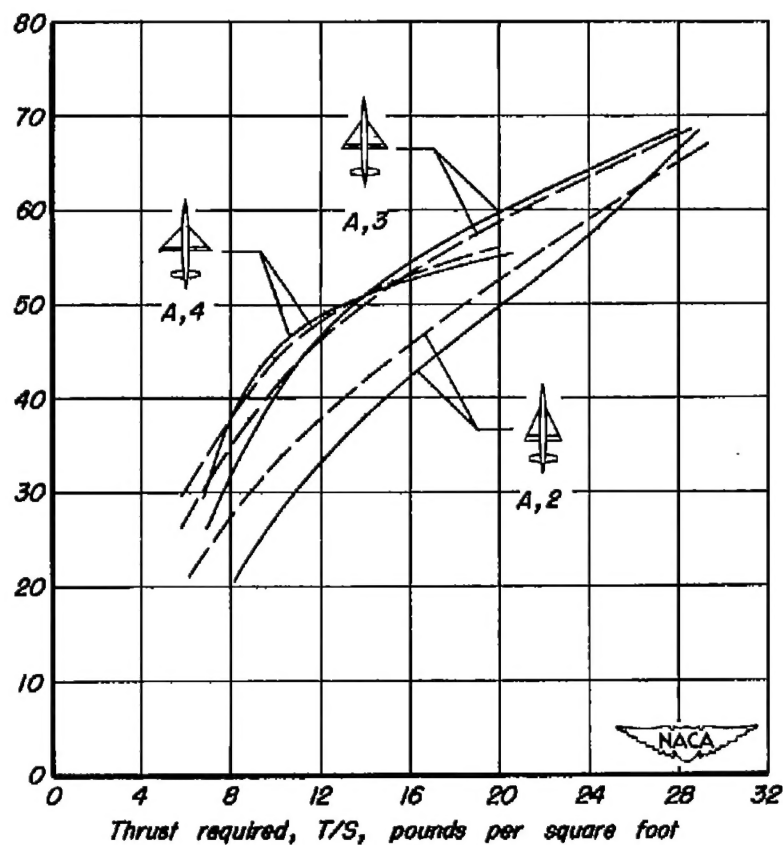
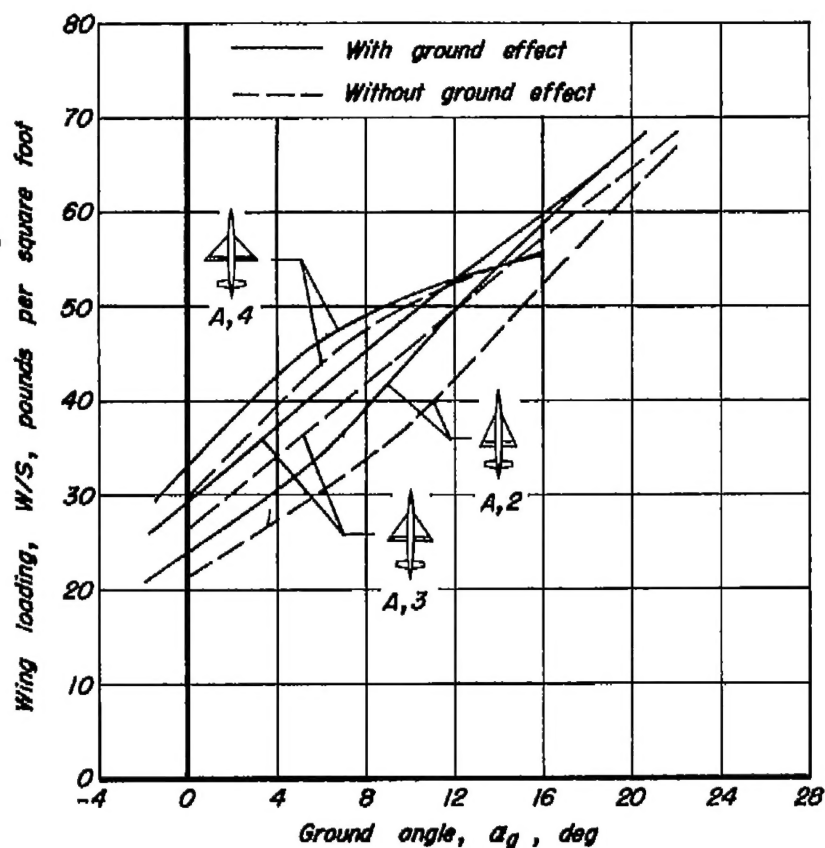


Figure 23.- Effect of proximity to the ground on the maximum wing loadings and thrust required for the three triangular wing models at a horizontal speed of 120 miles per hour and zero sinking speed. Gear down;  $\delta_F$ ,  $40^\circ$ ;  $h$ , 7 ft;  $(dc_m/dc_L)_{C_L} = 0$ ,  $-0.06$ .